UNIVERSITY OF OSLO
Department of Geosciences
MetOs Section

Mean currents induced by shelf waves along the western coast of Norway

Master thesis in Geosciences Meteorology and Oceanography

Magnus Drivdal

23rd June 2010

Abstract

Based on linear shallow water theory for a uniformly rotating, homogeneous ocean, the properties of freely propagating shelf waves are investigated, applying the rigid lid approximation. Applied to the Norwegian shelf, the ocean depth is allowed to vary in the direction normal to the coast, in two different models of the bottom topography. The stream function solutions of the resulting vorticity equations are found, the dispersion diagrams are plotted, and the kinematic properties of the waves are discussed.

The linear theory derived for the shelf waves is applied in an attempt to find the wave-induced mean currents along the western coast of Norway. First, the friction is neglected, and the second-order Stokes drift inherent in the wave motion is found. Secondly, to take the effect of dissipation into account, the linear analysis is redone, including friction in the momentum equation. The waves are in this case assumed to be long, which simplifies the analysis considerably. The resulting, damped solutions are used to calculate the wave-induced, non-linear forcing terms in the vertically integrated momentum and continuity equations. This yields a set of equations that are solved for the total mean Lagrangian volume flux.

Aknowledgements

I would like to thank my supervisor Jan Erik Weber for his patient and encouraging guidance throughout the work with this thesis. I would also like to thank all the helpful and supporting people of MetOs section, especially my co-supervisor Lars Petter Røed for helpful input.

Also, big thanks to all my fellow students for contributing intellectually through discussions and practical help, and socially by support and encouragement.

Contents

List of Figures

Chapter 1

Introduction

As shown for instance by LeBlond and Mysak (1978), the trapping of wave energy can occur where there are changes in bottom topography. In an area with sloping bottom, it is the displacement of particles perpendicular to the bottom contours that generates waves.
These waves are called escarpment waves, and they arise as a consequence of the conservation of potential vorticity. When a vertical fluid column is stretched or squeezed in a motion back and forth across the bottom contours, the relative vorticity changes periodically in time. In the case of the escarpment being a shelf, these waves are called shelf waves, and this type of waves will be the focus of this thesis. Shelf waves have large periods and wavelengths, they depend both on the depth variations and on the earth's rotation and are highly rotational (Mysak, 1980a). In a given hemisphere the shelf waves can only propagate in one direction relative to the shelf.

When working with wave motion in fluids, it is often assumed that the individual particles move in closed trajectories. While this is correct in the linear approach, it was shown by Stokes (1847) that non-linearly the particle trajectories are in fact not closed, and that the particles have a slow net drift in the wave propagation direction. In this manner the waves induce a mean current in the medium through which they propagate. The Stokes drift is essentially a direct result of the periodic nature of the waves, and is basically independent of friction. Taking account of the viscosity, it was shown by Longuet-Higgins (1953) that due to friction, lost wave momentum is transferred to mean Eulerian currents. To find the total wave-induced current, or the total Lagrangian drift, both the Stokes drift and the mean Eulerian currents need to be considered.

In this thesis the total Lagrangian drift induced by shelf waves will be studied, applied to the western coast of Norway. Along the Norwegian shelf these waves can only propagate northwards, with the shallower water to

the right, and one goal of this thesis is to investigate if this leads to a steady net mass transport along the shelf in one particular direction. Such a drift can have an impact on the climate due to the transport of heat and salt to the Arctic, and it will have implications for the transport of organic matter and pollution.

To study the Shelf waves, the bottom topography will be represented by both a step-profile of the shelf, as done by Martinsen et al. (1979), and by an exponential profile, as done by Buchwald and Adams (1968), and the resulting Stokes drift for both profiles will be compared.

This thesis will have the following structure: In chapter 2 the vorticity equation is derived, based on shallow water theory, and applying the f-plane and the rigid-lid approximations. In chapter 3 the different models for the bottom topography are introduced, and the stream function solutions of the vorticity equation are found. Furthermore, the dispersion diagrams are plotted, and some kinematic properties of the waves are discussed. Chapter 4 deals with the nonlinear properties of the shelf waves, and results for the different shelf profiles are discussed.

Chapter 2

Linear theory for Shelf waves

Starting with the shallow water equations, considering motion on an f-plane, the vorticity equation for shelf waves will be derived in this chapter, laying the basis for subsequent chapters.
A map of the western coast of Norway, which also displays the bottom topography, is shown in figure 2.1 on the following page.
To model the shelf waves outside the western coast of Norway, a straight coastline bounding an infinite ocean will be considered. When modelling the interior shelf, the shelf will be bounded by an infinite ocean of constant depth on both sides. The axes are chosen like in figure 2.2 on page 5, with the x axis pointing northwards along the coast, and the y axis normal to it. The depth H is a function of y only, and the width of the shelf is constant B. In this chapter we will work with a general $H(y)$, which will, together with B, be specified in the next chapter.

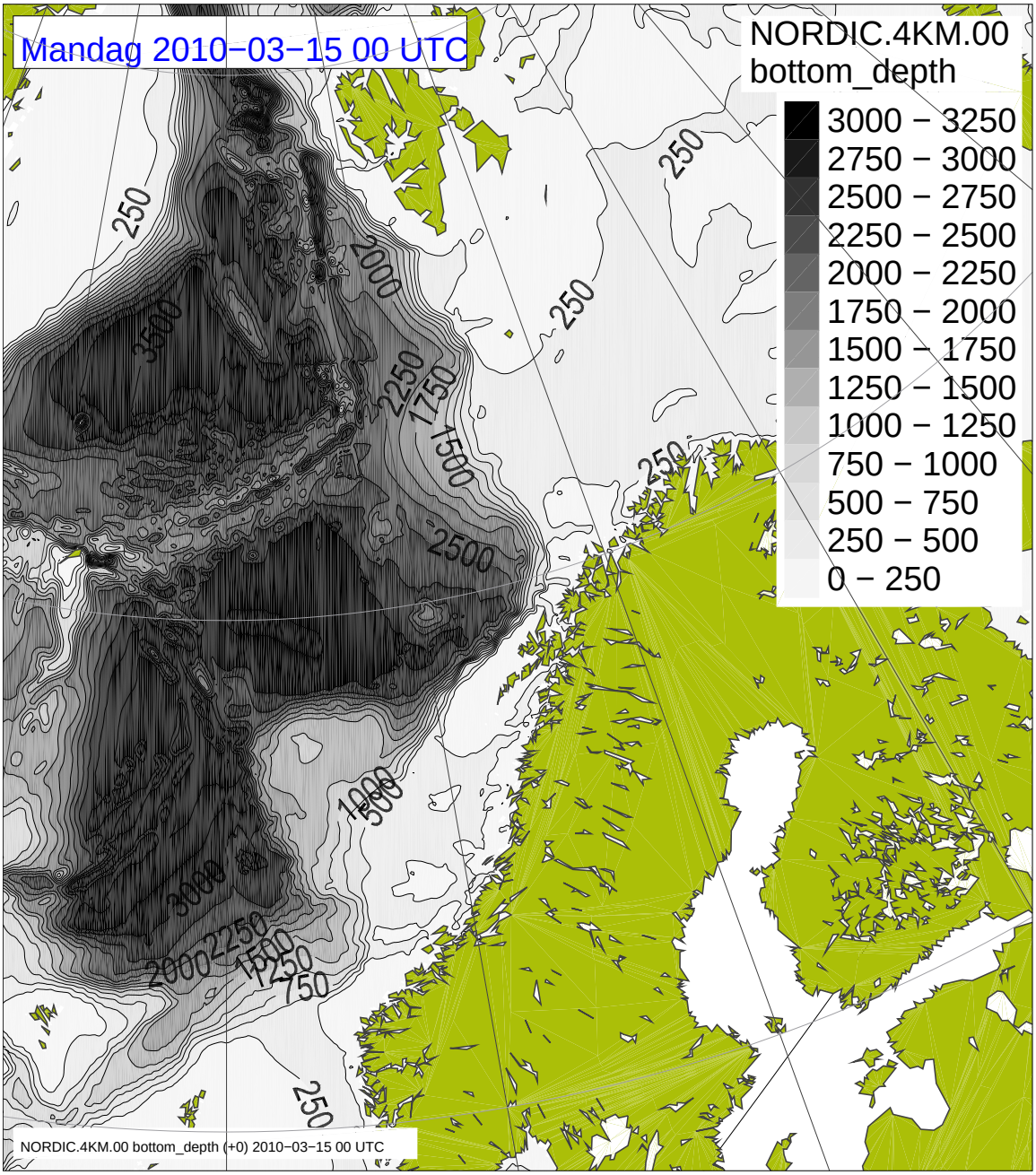

Figure 2.1: The western coast of Norway, and the bottom topography

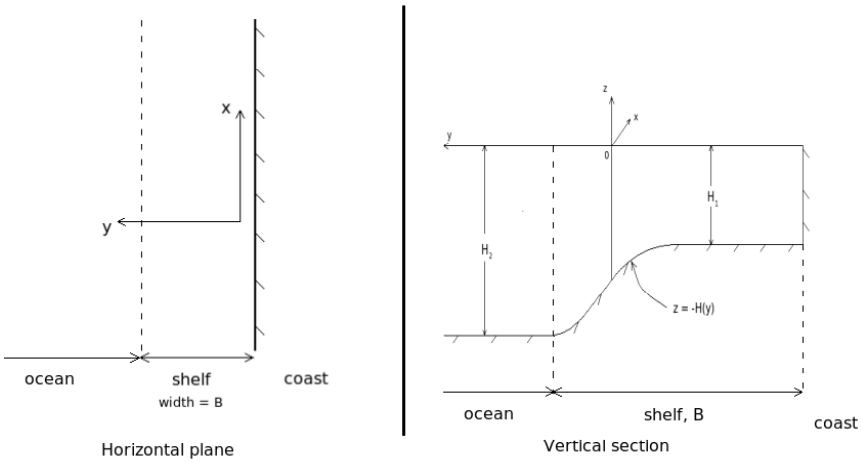

Figure 2.2: The shelf model; H(y) is the depth, B is the shelf width

2.1 Basic equations

Shallow water dynamics
The motion of a fluid is described by the momentum equation

$$\frac{D\vec{v}}{dt} = -f\vec{k} \times \vec{v} - \frac{1}{\rho}\nabla p - g\vec{k} + \vec{F}(\vec{v}), \tag{2.1.1}$$

where $f = 2\Omega sin\varphi$ is the Coriolis parameter, g is the acceleration due to gravity and $\vec{F}$ denotes the friction force on a fluid particle. The tidal force and the effect of the centrifugal force on the apparent gravity have been neglected.
In a fluid of constant density, the continuity equation becomes

$$\nabla \cdot \vec{v} = 0 \tag{2.1.2}$$

The basis for shallow water dynamics is to assume that the horizontal length scale of motion is much larger than the vertical length scale, which makes the main balance in the vertical momentum equation (2.1.1) hydrostatic, i.e.

$$\frac{\partial p}{\partial z} = -\rho g \tag{2.1.3}$$

By also assuming that the density is constant (homogeneous ocean) and by disregarding the friction, the momentum equation (2.1.1) simplifies, and

the horizontal components become

$$\frac{\partial u}{\partial t} + u\frac{\partial u}{\partial x} + v\frac{\partial u}{\partial y} - fv = -g\frac{\partial \eta}{\partial x} - \frac{1}{\rho}\frac{\partial P_S}{\partial x}, \tag{2.1.4}$$

$$\frac{\partial v}{\partial t} + u\frac{\partial v}{\partial x} + v\frac{\partial v}{\partial y} + fu = -g\frac{\partial \eta}{\partial y} - \frac{1}{\rho}\frac{\partial P_S}{\partial y}, \tag{2.1.5}$$

where P_S denotes the pressure at the surface, and η the surface elevation. The vertical velocity can be avoided in the continuity equation (2.1.2) by integrating it in the vertical, applying the kinematic boundary conditions at the free surface and at the bottom. Following Gill (1982) the kinematic boundary condition at the surface can be written as

$$w = \frac{D\eta}{dt}, \quad z = \eta, \tag{2.1.6}$$

while the kinematic boundary condition at the bottom is that of no normal flow, i.e.

$$w = -u\frac{\partial H}{\partial x} - v\frac{\partial H}{\partial y}, \quad z = -H \tag{2.1.7}$$

Integrating (2.1.2) with respect to depth, using the boundary conditions (2.1.6) and (2.1.7), then yields

$$\frac{\partial \eta}{\partial t} + \frac{\partial}{\partial x}\int_{-H}^{\eta} u dz + \frac{\partial}{\partial y}\int_{-H}^{\eta} v dz = 0 \tag{2.1.8}$$

With u and v independent of z, (2.1.8) becomes

$$\frac{\partial \eta}{\partial t} + \frac{\partial}{\partial x}\left(u(H+\eta)\right) + \frac{\partial}{\partial y}\left(v(H+\eta)\right) = 0 \tag{2.1.9}$$

The equations (2.1.4), (2.1.5) and (2.1.9) are often referred to as the shallow water equations.
The generation of shelf waves has been investigated in an article by Gill and Schumann (1974), and will not be addressed here, so the forcing terms in (2.1.4) and (2.1.5) will be neglected in the subsequent analysis. With this, linearizing the equations (2.1.4), (2.1.5) and (2.1.9) results in:

$$\frac{\partial u}{\partial t} - fv = -g\frac{\partial \eta}{\partial x} \tag{2.1.10}$$

$$\frac{\partial v}{\partial t} + fu = -g\frac{\partial \eta}{\partial y} \tag{2.1.11}$$

$$\frac{\partial \eta}{\partial t} + \frac{\partial}{\partial x}(uH) + \frac{\partial}{\partial y}(vH) = 0 \tag{2.1.12}$$

Important assumptions
Before we go any further in the analysis, it is convenient to make two important approximations. One is the assumption that

$$f = \text{const.}, \tag{2.1.13}$$

which is often refferred to as the f-plane approximation. Buchwald and Adams (1968) have shown that the β-effect can indeed be neglected to a good approximation for the case of an exponential shelf model. Here we will be content by simply stating that for the periods (1-10 days), shelf-width ($\sim$ 100 km) and wavelengths of interest, the β-effect is negligible, and hence the f-plane approximation is good.
The second approximation is that the term $(\partial\eta/\partial t)$ in (2.1.12) can be neglected, enabling the introduction of a stream function. This is often called the rigid-lid approximation, and to show under what conditions this approximation can be made, u and v are eliminated from equations (2.1.10) to (2.1.12).
Defining

$$\chi = \frac{\partial^2}{\partial t^2} + f^2,$$

and taking $\frac{\partial}{\partial t}(2.1.10) + f(2.1.11)$, $-f(2.1.10) + \frac{\partial}{\partial t}(2.1.11)$ and $\chi(2.1.12)$ yields the three equations

$$\chi u = -g\left(\frac{\partial^2\eta}{\partial x\partial t} + f\frac{\partial\eta}{\partial y}\right), \tag{2.1.14}$$

$$\chi v = -g\left(\frac{\partial^2\eta}{\partial y\partial t} - f\frac{\partial\eta}{\partial x}\right), \tag{2.1.15}$$

$$\chi\frac{\partial\eta}{\partial t} + \chi\frac{\partial}{\partial x}(uH) + \chi\frac{\partial}{\partial y}(vH) = 0 \tag{2.1.16}$$

Taking $\frac{\partial}{\partial x}(H\cdot(2.1.14)) + \frac{\partial}{\partial y}(H\cdot(2.1.15)) - (2.1.16)$, we get, after some algebra

$$\frac{\partial}{\partial t}\left[\frac{\partial}{\partial x}\left(H\frac{\partial\eta}{\partial x}\right) + \frac{\partial}{\partial y}\left(H\frac{\partial\eta}{\partial y}\right) - \frac{1}{g}\chi\eta\right] - f\frac{dH}{dy}\frac{\partial\eta}{\partial x} = 0, \tag{2.1.17}$$

If the term $g^{-1}\chi(\partial\eta/\partial t)$ can be neglected in (2.1.17), the term $(\partial\eta/\partial t)$ can be neglected in (2.1.12), which means that the flow is assumed horizontally non-divergent. To identify the relative size of the terms in (2.1.17), the equation is scaled using the following dimensionless variables

$$\hat{x} = \frac{x}{L}, \quad \hat{y} = \frac{y}{B}, \quad \hat{t} = \frac{t}{T}, \quad \hat{\eta} = \frac{\eta}{\eta_c}, \quad \hat{H} = \frac{H}{H_c}, \tag{2.1.18}$$

where B is the width of the shelf (see figure 2.2), H_c is the depth averaged some way over the shelf, η_c is some characteristic surface elevation, T represents the wave period and L represents the wavelength. Inserting (2.1.18) into (2.1.17) gives the dimensionless equation

$$\begin{aligned}&\frac{\partial}{\partial\hat{t}}\left[\frac{H_c\eta_c}{L^2}\frac{\partial}{\partial\hat{x}}\left(\hat{H}\frac{\partial\hat{\eta}}{\partial\hat{x}}\right) + \frac{H_c\eta_c}{B^2}\frac{\partial}{\partial\hat{y}}\left(\hat{H}\frac{\partial\hat{\eta}}{\partial\hat{y}}\right) - \frac{\eta_c}{g}\hat{\chi}\hat{\eta}\right]\\ &- \frac{fT\eta_c}{L}\left(H'\frac{\partial\hat{\eta}}{\partial\hat{x}}\right) = 0,\end{aligned} \tag{2.1.19}$$

where $H' = dH/dy$ has been kept as a parameter in the last term since it is already dimensionless and

$$\hat{\chi} = \frac{1}{T^2}\frac{\partial^2}{\partial \hat{t}^2} + f^2$$

Typically the long-shore length scale L, which represents the wavelength of the shelf waves, is larger than the shelf width B, and hence the second term in (2.1.19) is larger than the first term. Here it suffices to say that for $L \geq B$, comparison of the three first terms in (2.1.19) gives the following condition for the neglect of $\partial\eta/\partial t$

$$\frac{H_c}{B^2} \gg \frac{1}{g}\left(\frac{1}{T^2} + f^2\right) \tag{2.1.20}$$

Like in the article by Buchwald and Adams (1968), the wave periods will be assumed to be larger than the inertial period, i.e. $T > 2\pi/f$, and (2.1.20) reduces to

$$\epsilon^2 = \frac{f^2 B^2}{g H_c} \ll 1, \quad or \quad \frac{B^2}{a^2} \ll 1, \tag{2.1.21}$$

where $a^2 = gH_c/f^2$ is the external, or barotropic, Rossby radius (LeBlond and Mysak, 1978). The parameter ϵ is the same as that used by Buchwald and Adams (1968); Gill and Schumann (1974).
By comparison of the third and fourth terms of (2.1.19) another condition for the rigid-lid approximation is that

$$T \gg \frac{fL}{gH'} \tag{2.1.22}$$

Since $L = 2\pi/k$ and $T = 2\pi/\omega$, (2.1.22) is equivalent to $c \equiv \omega/k \ll gH'/f$, which is used by Gill and Schumann (1974).
In summary, the conditions (2.1.21) and (2.1.22) mean that neglect of $\partial\eta/\partial t$ in the continuity equation requires that the shelf width is much smaller than the Rossby radius and that the waves considered must have long wave periods. The last requirement is fulfilled for most shelf waves, since they typically have periods of several days (Mysak, 1980b).
For the Norwegian shelf, with $B \sim 100$ km, (2.1.21) is satisfied, and the shallow water continuity equation (2.1.12) becomes

$$\frac{\partial}{\partial x}(uH) + \frac{\partial}{\partial y}(vH) = 0 \tag{2.1.23}$$

2.2 The vorticity equation

Using the equations from the previous subsection, a differential equation describing continental shelf waves will here be derived. The coordinate system is as described in figure 2.2 on page 5, with bottom slope $H = H(y)$. By taking the negative y-derivative of (2.1.10) plus the x-derivative of (2.1.11), which means that we operate the curl on the vector equation, η is eliminated from the system and we get the vorticity equation:

$$\frac{\partial}{\partial t}\left(\frac{\partial v}{\partial x} - \frac{\partial u}{\partial y}\right) + f\left(\frac{\partial u}{\partial x} + \frac{\partial v}{\partial y}\right) = 0 \tag{2.2.1}$$

The continuity equation (2.1.23) can be rewritten:

$$\frac{\partial u}{\partial x} + \frac{\partial v}{\partial y} = -\frac{1}{H}\frac{dH}{dy}v \tag{2.2.2}$$

(2.2.2) into (2.2.1) gives

$$\frac{\partial}{\partial t}\left(\frac{\partial v}{\partial x} - \frac{\partial u}{\partial y}\right) - \frac{f}{H}\frac{dH}{dy}v = 0 \tag{2.2.3}$$

The simplified continuity equation (2.1.23) can also be used to introduce a stream function:

$$Hu = -\frac{\partial \psi}{\partial y}, \quad Hv = \frac{\partial \psi}{\partial x} \tag{2.2.4}$$

(2.2.4) into (2.2.3) then gives

$$\frac{\partial}{\partial t}\left[\frac{\partial}{\partial x}\left(\frac{1}{H}\frac{\partial \psi}{\partial x}\right) + \frac{\partial}{\partial y}\left(\frac{1}{H}\frac{\partial \psi}{\partial y}\right)\right] - \frac{f}{H^2}\frac{dH}{dy}\frac{\partial \psi}{\partial x} = 0 \tag{2.2.5}$$

Assuming a traveling wave solution of the form

$$\psi = F(y)\exp(i(kx - \omega t)), \tag{2.2.6}$$

we find that F must satisfy

$$\left(\frac{F'}{H}\right)' - \left(\frac{k^2}{H} - \frac{fk}{\omega}\frac{H'}{H^2}\right)F = 0, \tag{2.2.7}$$

where $F' = dF/dy$ and $H' = dH/dy$.
Since this differential equation for F has non-constant coefficients, it is problematic to solve for a general bottom topography $H(y)$. In the next chapter this problem will be dealt with by choosing two different types of bottom topography, a step shelf and an exponential shelf.

2.3 The mechanism for propagation of shelf waves

Equation (2.2.3) really states the conservation of potential vorticity. Before we go any further in the analysis, the conservation of potential vorticity theorem can be used to get a more intuitive and qualitative understanding of the mechanism that drives the shelf waves. In the case of negligible surface elevation (i.e. under the rigid lid approximation), the potential vorticity, Q, is given by

$$Q = \frac{f + \zeta}{H}, \tag{2.3.1}$$

where $\zeta \equiv \partial v/\partial x - \partial u/\partial y$ is the relative vorticity, f is the planetary vorticity and H is the depth. The conservation of potential vorticity can then be stated by

$$\frac{DQ}{dt} = 0 \tag{2.3.2}$$

It can easily be verified, assuming that f is constant and linearizing, that 2.3.2 is equivalent to 2.2.3. Consider a particle that moves from deep water to shallower water, the conservation of potential vorticity then implies that ζ in (2.3.1) must decrease to compensate for the decrease in H. In other words particles moving into shallower water acquire anticyclonic relative vorticity, and particles moving into deeper water acquire cyclonic relative vorticity. This fact can be used to investigate the propagation of shelf waves, analog to the way Longuet-Higgins (1965) explained the westward propagation of planetary waves. Now, consider a line of particles lying originally along a depth contour as shown in figure 2.3 on the next page, and suppose they are displaced so as to lie along a sine-curve. The particles now displaced to the shallower water from the mean position will have acquired anticyclonic relative vorticity, while the particles displaced to the deeper water will have acquired cyclonic relative vorticity. With velocities towards deeper water just to the right of the crest and towards shallower water just to the left, the phase of the wave tends to drift in the direction with the shallower water to the right. This fact is illustrated by the arrows in figure 2.3.

This simple and qualitative approach illustrates how the vorticity drives the waves, and intuitively explains that the waves must propagate with the shallower water to the right, a fact that we will later find from the dispersion relation.

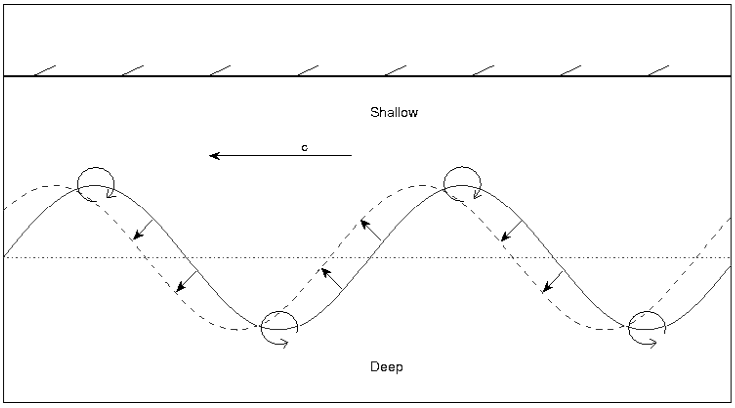

Figure 2.3: The mechanism for propagation of shelf waves. The line of particles (solid line) moves to the position of the dashed line, as indicated by the arrows. (Similar to Gill (1982), fig. 10.18; Longuet-Higgins (1965), fig. 13.)

Chapter 3

Applications to specific bottom topography

To study shelf waves off the western coast of Norway and over the interior shelf north of Norway, the bottom topography, the value of the Coriolis parameter and the size of the shelf must be specified. In an earlier study by Martinsen et al. (1979), the Norwegian shelf was modelled by a step-function, and characteristic values for the depth and shelf width were introduced. In this chapter, as a first approach, the continental shelf will be modelled in the same way. As a more realistic model, an exponential shelf profile will also be used, similar to the one used by Buchwald and Adams (1968) in a study of shelf waves off the East Australian coast. The exponential shelf profile will also be used to study shelf waves over the interior shelf north of Norway, where there is no coastal boundary. To be able to relate the two models for the continental shelf, the exponential profile will be fitted in a way such that the cross-sectional area under the exponential shelf profile equals the area under the step-shelf (see figure 3.1 below). The depth at the coast (H_1) and the depth in deep ocean (H_2) will be the same in both models, with values taken from Martinsen et al. (1979). The width of the step-shelf, from now on denoted by B_1, will also be the same as in this article, while the width of the exponential shelf, B_2, will be calculated.
From Martinsen et al. (1979) we have the following values for the Norwegian shelf:

$$H_1 = 250 \text{ m}, \quad H_2 = 2500 \text{ m}, \quad B_1 = 105 \text{ km}, \quad f = 1.3 \cdot 10^{-4} \text{ s}^{-1} \quad (3.0.1)$$

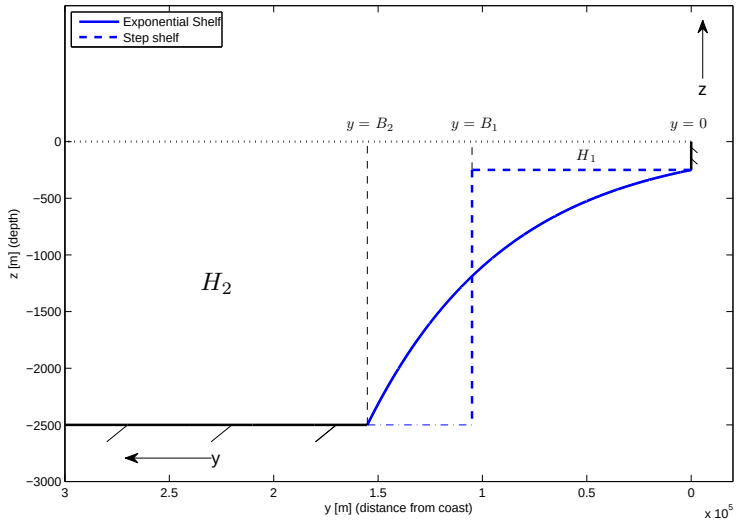

Figure 3.1: Step-shelf and exponential shelf model for the continental shelf of Norway

3.1 The continental shelf of Norway

3.1.1 The step shelf model

As a first attempt, the continental shelf will be modelled as a step-function as seen in figure 3.2 on the following page. The depth is then simply given by

$$H = \begin{cases} H_1, & 0 \leq y \leq B_1 \\ H_2, & y > B_1 \end{cases} \tag{3.1.1}$$

For this type of topography, where the depth is constant on both sides of the shelf, equation (2.2.7) on page 9 simplifies to

$$F_i'' - k^2 F_i(y) = 0, \quad i = 1, 2, \tag{3.1.2}$$

where the subscript denotes which side of the shelf that is considered. (3.1.2) is a second order, linear and ordinary differential equation with constant coefficients, which can easily be solved. The boundary condition at the coast is that there can be no mass flux into the coast, i.e. $Hv = 0$. From (2.2.4) and (2.2.6) this translates to

$$F_1 = 0, \quad y = 0 \tag{3.1.3}$$

In the deep ocean, far from the coast, the boundary condition is

$$F_2 \to 0 \quad as \quad y \to \infty \tag{3.1.4}$$

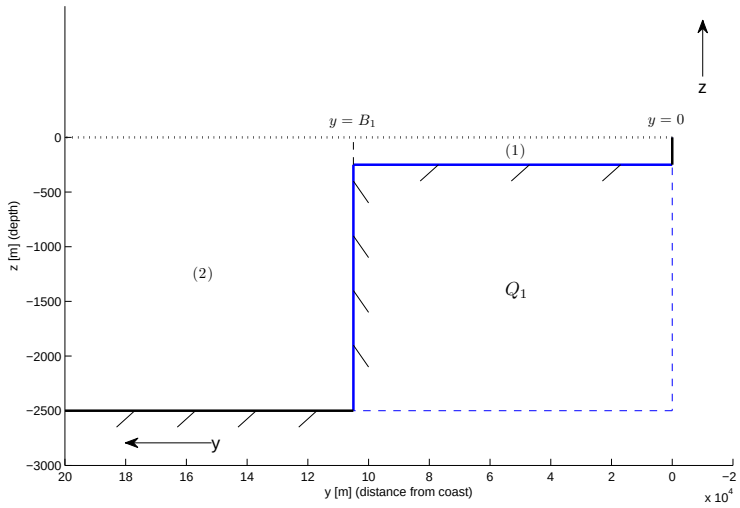

Figure 3.2: Step-shelf model, areas with depths H_1 and H_2 are denoted by (1) and (2), respectively. Q_1 is the cross-section of the shelf.

At the step ($y = B_1$), the volume flux must be continuous, so a third boundary condition is:

$$v_1 H_1 = v_2 H_2, \quad y = B_1, \tag{3.1.5}$$

which means that ψ_x, and hence also ψ is continuous for $y = B_1$.
A general solution to (3.1.2) is:

$$F_i = A_i e^{ky} + C_i e^{-ky}, \quad i = 1, 2 \tag{3.1.6}$$

Using the boundary condition at the coast, (3.1.3), in (3.1.6) we find that $C_1 = -A_1$, and we have that

$$F_1 = D_1 \sinh(ky), \quad (D_1 = 2A_1) \tag{3.1.7}$$

Furthermore, considering positive k and using (3.1.4) in (3.1.6), we find that A_2 must be zero, and that

$$F_2 = C_2 e^{-ky} \tag{3.1.8}$$

Continuous ψ at $y = B_1$ is satisfied if

$$C_2 = D_1 \sinh(kB_1) e^{kB_1}, \tag{3.1.9}$$

and we get:

$$F = \begin{cases} D_1 \sinh(ky) & 0 \leq y \leq B_1 \\ D_1 \sinh(kB_1) e^{-k(y-B_1)} & y > B_1 \end{cases} \tag{3.1.10}$$

which inserted into (2.2.6) on page 9 gives

$$\psi = \begin{cases} D_1 \sinh(ky) e^{i(kx-\omega t)} & 0 \leq y \leq B_1 \\ \\ D_1 \sinh(kB_1) e^{-k(y-B_1)} e^{i(kx-\omega t)} & y > B_1 \end{cases} \tag{3.1.11}$$

The dispersion relation

In addition to the volume flux, the pressure in the fluid must also be continuous at $y = B_1$. In the absence of friction, the linearized x-component of the momentum equation (2.1.1) on page 5 becomes:

$$\frac{\partial p}{\partial x} = -\rho \left(\frac{\partial u}{\partial t} - fv \right) = -\frac{\rho}{H} \left(\frac{\partial}{\partial t}(Hu) - fHv \right) \tag{3.1.12}$$

Assuming $p = P(y) \exp(i(kx - \omega t))$, using (2.2.4) and (2.2.6) we find that

$$P = \rho \left(-\frac{\omega F'}{kH} + \frac{fF}{H} \right) \tag{3.1.13}$$

Using (3.1.10) in (3.1.13), continuity of the pressure at $y = B_1$ yields the dispersion relation

$$\frac{\omega}{f} = \frac{H_2 - H_1}{H_2 \coth(kB_1) + H_1} \tag{3.1.14}$$

Since $H_2 > H_1$ and $f > 0$ in the northern hemisphere, the frequency $\omega > 0$, and hence the wave propagates in the positive x-direction with the shallow water to the right. Furthermore, from (3.1.14), it is evident that the group and phase velocities are always in the same direction.

Using the shelf width B_1 as the unit length, we can plot the dispersion ratio $\sigma = \omega/f$ against the dimensionless wavenumber kB_1:

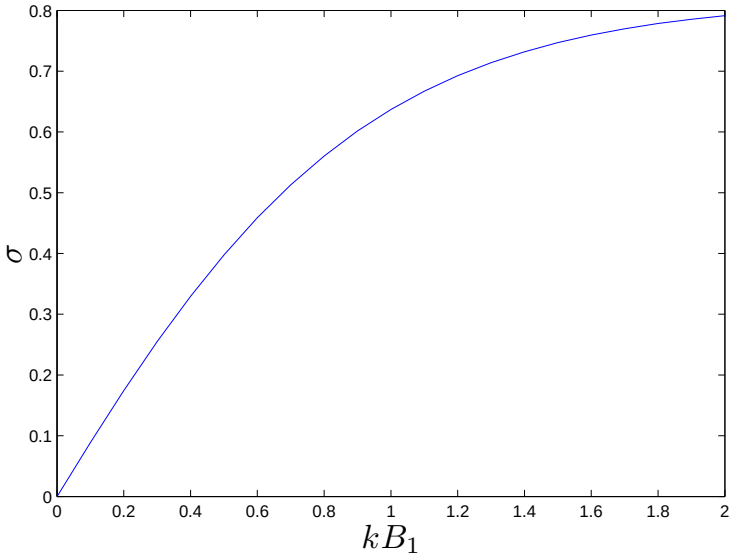

Figure 3.3: The dispersion ratio plotted against kB_1 for the step shelf

From (3.1.14) and figure 3.3 it is clear that the frequency ω increases monotonically with k and that it is always subinertial, i.e. $|\omega/f| < 1$. It can also bee seen from equation (3.1.14) that, in the short-wave limit

$$\frac{\omega}{f} \to \frac{H_2 - H_1}{H_2 + H_1} \quad as \quad kB_1 \to \infty, \tag{3.1.15}$$

which is identical to the dispersion relation for double Kelvin waves along an abrupt escarpment (see for instance LeBlond and Mysak (1978)). In this limit, the group velocity is identically zero, and no energy propagates along the shelf (LeBlond and Mysak, 1978). Since this thesis will focus on waves having wavelengths longer than the shelf width, it is more interesting to see that at small wave numbers

$$\frac{\omega}{f} \to (H_2 - H_1)kB_1, \quad as \quad kB_1 \to 0 \tag{3.1.16}$$

From (3.1.16) we see that the phase and group velocity become equal for long waves, i.e. the waves become nondispersive. While Martinsen et al. (1979) find two wave modes, the shelf wave and the Kelvin-type edge wave, the solution here has only one mode. This is because of the assumption that $\partial\eta/\partial t$ can be neglected in the continuity equation (2.1.12), made in the previous chapter, which filters out the Kelvin waves.

3.1.2 The exponential shelf model

While the step profile that was used in the previous section made it simple to solve (2.2.7), the singular depth variation filters out all higher shelf wave modes (Mysak, 1980b). To study the modal structure of the shelf waves, we will in this section use a profile of the form

$$H(y) = \begin{cases} H_1 e^{2by}, & 0 \leq y < B_2 \\ H_2, & y > B_2, \end{cases} \tag{3.1.17}$$

where

$$H_2 = H_1 e^{2bB_2}, \tag{3.1.18}$$

An essential quality of this exponential shelf profile, that was first studied by Buchwald and Adams (1968), is that the depth is continuous at the shelf edge, where $y = B_2$ (see figure 3.4). In the further analysis of this section the article of Buchwald and Adams (1968) will be followed, but working with wavesolutions of the form

$$\psi = H^{\frac{1}{2}}\phi(y)\exp(i(kx - \omega t)), \tag{3.1.19}$$

as done by Gill (1982). Choosing wavesolutions of this particular form, the first order derivatives of ϕ are avoided when inserting into (2.2.5) on page 9.

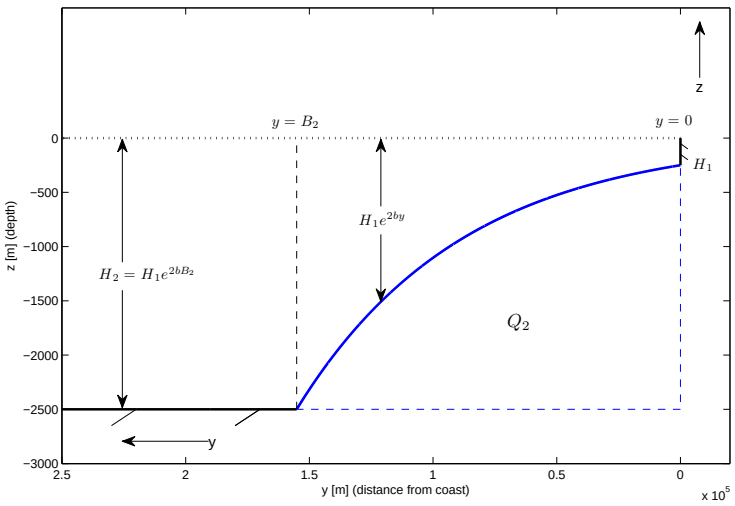

Figure 3.4: Exponential shelf model, the x-axis pointing northwards along the coast. Q_2 is the cross-section of the shelf.

To make sure that the area under the exponential shelf, Q_2 in figure 3.4, is

the same as the area under the step shelf, Q_1 in figure 3.2 on page 14, we need to determine values for B_2 and b so that both (3.1.18) and

$$Q_1 = Q_2, \tag{3.1.20}$$

are satisfied.
Rearranging (3.1.18) we can write $2b$ as a function of B_2

$$2b = \frac{1}{B_2} \cdot (\ln(H_2) - \ln(H_1)) \tag{3.1.21}$$

The areas can easily be found by simple geometry:

$$Q_1 = (H_2 - H_1) \cdot B_1, \tag{3.1.22}$$

$$Q_2 = H_2 \cdot B_2 - \int_0^{B_2} H_1 e^{2by}\, dy = H_2 \cdot B_2 - \frac{H_1}{2b}\left(e^{2bB_2} - 1\right), \tag{3.1.23}$$

and by using this in (3.1.20), we get that

$$(H_2 - H_1) \cdot B_1 = H_2 \cdot B_2 - \frac{H_1}{2b}\left(e^{2bB_2} - 1\right) \tag{3.1.24}$$

Using (3.1.21), (3.1.24) can be solved for B_2:

$$B_2 = \frac{(H_2 - H_1) \cdot B_1}{H_2 - \frac{H_2 - H_1}{\ln(H_2) - \ln(H_1)}} \tag{3.1.25}$$

Inserting the values from (3.0.1) into (3.1.25), the approximate value for B_2 becomes

$$B_2 = 155 \text{ km}, \tag{3.1.26}$$

and from (3.1.21) we then have approximately that

$$2b = 1.49 \cdot 10^{-5}\ \text{m}^{-1} \tag{3.1.27}$$

Together with (3.0.1), (3.1.26) and (3.1.27) provide the values that will later be needed to discuss the dispersion relation.
Inserting (3.1.19) into (2.2.5) on page 9 we get, after some algebra:

$$\frac{d^2\phi}{dy^2} + \left[\frac{d}{dy}\left(\frac{1}{2H}\frac{dH}{dy}\right) - \left(\frac{1}{2H}\frac{dH}{dy}\right)^2 - k^2 + \frac{fk}{\omega}\frac{1}{H}\frac{dH}{dy}\right]\phi = 0 \tag{3.1.28}$$

Let area 1, denoted by a subscript 1, be $0 \leq y < B_2$. Insertion from (3.1.17) into (3.1.28) then gives

$$\frac{d^2\phi_1}{dy^2} + \left[-b^2 - k^2 + \frac{2fkb}{\omega}\right]\phi_1 = 0 \tag{3.1.29}$$

As with the Step-shelf, the boundary condition at the coast must be that of no mass flux into the coast. Here this translates to

$$\phi_1 = 0, \quad y = 0 \tag{3.1.30}$$

From this we realize that ϕ_1 must be proportional to $\sin(ly)$, and hence a general solution to (3.1.29) is

$$\phi_1 = A_1 \sin(ly), \tag{3.1.31}$$

provided that

$$l = \sqrt{-b^2 - k^2 + \frac{2fkb}{\omega}} \tag{3.1.32}$$

By insertion of H_2 from (3.1.17) into (3.1.28), we find that the differential equation in area 2 simplifies to

$$\frac{d^2\phi_2}{dy^2} - k^2\phi_2 = 0, \tag{3.1.33}$$

with general solution

$$\phi_2 = A_2 e^{-ky} + A_3 e^{ky}. \tag{3.1.34}$$

To avoid a solution that grows beyond bonds as $y \to \infty$, we must have that $A_3 = 0$, and hence

$$\phi_2 = A_2 e^{-ky} \tag{3.1.35}$$

From (3.1.31), (3.1.35) and (3.1.19) we now have

$$\psi = \begin{cases} A_1 H_1^{\frac{1}{2}} e^{by} \sin(ly) e^{i(kx-\omega t)}, & 0 \le y < B_2 \\ \\ A_2' H_1^{\frac{1}{2}} e^{-ky} e^{i(kx-\omega t)}, & y > B_2, \end{cases} \tag{3.1.36}$$

where $A_2' = \exp(bB_2)A_2$.
The volume flux, and thereby also ψ, must be continuous at $y = B_2$ as argued in the discussion about the step-shelf. Continuity of ψ in (3.1.36) gives that

$$A_1 e^{bB_2} \sin(lB_2) = A_2' e^{-kB_2}, \tag{3.1.37}$$

which is satisfied if

$$A_1 = D_2 e^{-bB_2} \quad \textit{and} \quad A_2' = D_2 e^{kB_2} \sin(lB_2). \tag{3.1.38}$$

Inserting (3.1.38) into (3.1.36) we then find that

$$\psi = \begin{cases} D_2 H_1^{\frac{1}{2}} e^{b(y-B_2)} \sin(ly) e^{i(kx-\omega t)}, & 0 \le y < B_2 \\ \\ D_2 H_1^{\frac{1}{2}} e^{k(B_2-y)} \sin(lB_2) e^{i(kx-\omega t)}, & y > B_2 \end{cases} \tag{3.1.39}$$

The dispersion relation

By rearranging (3.1.32) we find that the dispersion ratio can be expressed by

$$\frac{\omega}{f} = \frac{2kb}{k^2 + l^2 + b^2}, \tag{3.1.40}$$

From (3.1.40) it is obvious that $\omega < f$, and we can find that the free wave speed is given by

$$c = \frac{\omega}{k} = \frac{2fb}{l^2 + b^2 + k^2} \tag{3.1.41}$$

This clearly shows that the direction of propagation depends on the sign of f, and the waves travel with shallow water to the right in the northern hemisphere. The value of l depends on how wide the region with exponentially varying depth is, i.e. the value of B_2, and also on the properties of the ocean seaward of that region (Gill, 1982).

To find the possible values of l, given a shelf profile like (3.1.17), another boundary condition at $y = B_2$ is needed. With the assumption of hydrostatic pressure distribution in the vertical, from equation (2.1.3) on page 5, the continuity of pressure at $y = B_2$ is equivalent to the continuity of surface elevation η. Using the definition of the stream function (2.2.4) on page 9 in the x-momentum equation (2.1.10) on page 6, assuming the wavelike form of (3.1.19), the surface elevation is given by

$$gH\eta = f\psi - \frac{\omega}{k}\frac{\partial \psi}{\partial y} \tag{3.1.42}$$

Hence, continuity of η also means that $\partial\psi/\partial y$ must be continuous at $y = B_2$, and by the use of (3.1.39) we then get the frequency equation

$$b\sin(lB_2) + l\cos(lB_2) = -k\sin(lB_2),$$

or, by rearranging

$$\tan(lB_2) = -\frac{l}{b+k} \tag{3.1.43}$$

The roots of the frequency equation (3.1.43) can be studied by considering the intersections of the graph of the left hand side and the right hand side. While the roots could also be found numerically, the graphical solutions are useful for finding starting points for a numerical iteration method (this has been used here when plotting the dispesion curves in figure 3.6 on page 23 and 3.10 on page 30). Using the shelf width as the unit of length, as done by Buchwald and Adams (1968), the dimensionless version of (3.1.43) becomes

$$\tan(\hat{l}) = -\frac{\hat{l}}{\hat{b}+\hat{k}} \quad , \tag{3.1.44}$$

where

$$\hat{l} = lB_2, \quad \hat{b} = bB_2, \quad \hat{k} = kB_2. \tag{3.1.45}$$

From (3.1.26) and (3.1.27) we have approximately that

$$\hat{b} = bB_2 = 1.15. \tag{3.1.46}$$

Following Buchwald and Adams (1968), the graphs of $M = \tan(\hat{l})$ and the straight line $M = -\hat{l}/(\hat{b} + \hat{k})$ can now be plotted (see figure 3.5).

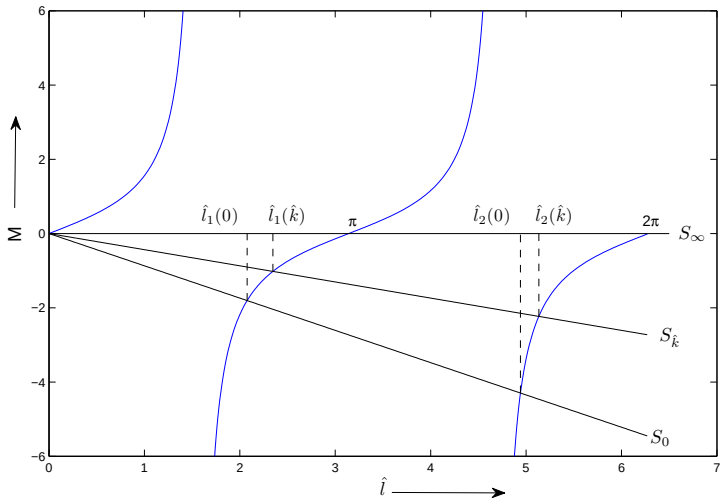

Figure 3.5: Intersections of $M = \tan(\hat{l})$ with $M = -\hat{l}/(\hat{b} + \hat{k})$

Here the straight lines are denoted by $S_{\hat{k}}$, and we see that as $\hat{k} \to \infty$, $S_{\hat{k}}$ tends to the $M = 0$ axis, so that the intersections are at $\hat{l} = n\pi$, where n is an integer. Furthermore, for $\hat{k} = 0$, S_0 has the equation $M = -\hat{l}/\hat{b}$. Here the intersections of S_0 with the graph of $\tan(\hat{l})$ are denoted by $\hat{l}_n(0)$, where the integer n denotes the appropriate branch of $\tan(\hat{l})$. From figure 3.5 it is then clear that $\hat{l}_n(0) \to (n - \frac{1}{2})\pi$ as $n \to \infty$. Figure 3.5 also illustrates that for each value of $\hat{k}$ there is an infinite number of intersections of $S_{\hat{k}}$ with $\tan(\hat{l})$ at $\hat{l} = \hat{l}_n(\hat{k})$, and that

$$(n - \frac{1}{2})\pi < \hat{l}_n(0) \leq \hat{l}_n(\hat{k}) \leq n\pi \tag{3.1.47}$$

Hence $\hat{l} = \hat{l}_n(\hat{k})$ is a continuous function of $\hat{k}$, increasing monotonously from $\hat{l}_n(0)$ to $n\pi$ as $\hat{k}$ varies form 0 to ∞. For the exponential shelf discussed

here, with $\hat{b}$ given by (3.1.46), we see from figure 3.5 on the preceding page that the approximate value of $\hat{l}_1(0)$ is 2.1, which means that $\hat{l}_1(\hat{k})$ increases from 2.1 to π as $\hat{k}$ varies from 0 to ∞.
Now equation (3.1.40) can be written in the form

$$\sigma_n = \frac{2\hat{b}\hat{k}}{\hat{k}^2 + \hat{l}_n^2 + \hat{b}^2}, \tag{3.1.48}$$

where σ is the frequency ratio ω/f, and $\hat{l}_n(\hat{k})$ is that branch of the solution of (3.1.44) which approaches $n\pi$ as $\hat{k} \to \infty$. Since $\hat{l}_n$ is upper and lower bound we have, from (3.1.47), that

$$\sigma_n \sim \frac{2\hat{b}}{\hat{k}}, \qquad \hat{k} \to \infty, \tag{3.1.49}$$

$$\sigma_n \sim \frac{2\hat{b}\hat{k}}{\hat{l}_n^2(0) + \hat{b}^2}, \qquad \hat{k} \to 0. \tag{3.1.50}$$

Each value of n represents a different branch of the function $\sigma(\hat{k})$, with $\hat{k}$ ranging from 0 to ∞. This will be called the 'nth mode' of the shelf waves. From (3.1.50) it is clear that for very long waves, σ_n is approximately linear in $\hat{k}$, and there is little dispersion. In this limit we then have from (3.1.50) that the phase velocity, $c \equiv \omega/k$, and the group velocity $c_g \equiv d\omega/dk$ are nearly constant and equal to

$$\frac{2\hat{b}f}{\hat{l}_n^2(0) + \hat{b}^2}, \tag{3.1.51}$$

or, in dimensional form

$$c = c_g = \frac{2bf}{l_n^2(0) + b^2}. \tag{3.1.52}$$

With $\hat{l}_1(0) = 2.1$, and by using (3.1.45) and (3.1.26), we find that $l_1(0)$ is approximately $1.35 \cdot 10^{-5} m^{-1}$. Using this in (3.1.52), together with the values of f and b from (3.0.1) and (3.1.27), respectively, we get that the local velocity of long shelf waves is approximately 8.1 m/s in the positive x-direction.
From (3.1.49) and (3.1.50), it is clear that the graph of $\sigma_n(\hat{k})$ has a maximum, as well as a point of inflexion. These can be located approximately by assuming that $\hat{l}_n$ is only a slowly varying function of $\hat{k}$, so that $\hat{l}_n'(\hat{k})$ is small (Buchwald and Adams, 1968). Then we can differentiate (3.1.48) with respect to $\hat{k}$, keeping $\hat{l}_n$ constant:

$$\sigma_n' = \frac{2\hat{b}\left(\hat{l}_n^2 + \hat{b}^2 - \hat{k}^2\right)}{\left(\hat{l}_n^2 + \hat{b}^2 + \hat{k}^2\right)^2} \tag{3.1.53}$$

By finding the value of $\hat{k}$ for which (3.1.53) is equal to zero, the maximum point is found, and we have

$$\hat{k}_n^* \approx \sqrt{\hat{l}_n^2 + \hat{b}^2}; \quad \sigma_n^* \approx \frac{\hat{b}}{\sqrt{\hat{l}_n^2 + \hat{b}^2}}; \quad \hat{k}_n^* \sigma_n^* = \hat{b}; \tag{3.1.54}$$

where $*$ is used to denote the coordinates of the maximum, and the value of $\hat{l}_n$ is somewhere between the limits $\hat{l}_n(0)$ and $n\pi$. The group velocity c_g is positive, and hence has the same sign as the phase speed c, for $\hat{k} < \hat{k}_n^*$. For $\hat{k} > \hat{k}_n^*$, c_g is negative, and has the opposite sign as c. At the point of inflexion, the group velocity has a turning point, and by taking $d/d\hat{k}$ of (3.1.53) equal to zero and solve for $\hat{k}$, we find that this point is approximately at

$$\hat{k} = \hat{k}_n^{**} \approx \sqrt{3\left(\hat{b}^2 + \hat{l}_n^2\right)} \tag{3.1.55}$$

In figure 3.6, the dispersion ratio σ is plotted for the three first modes.

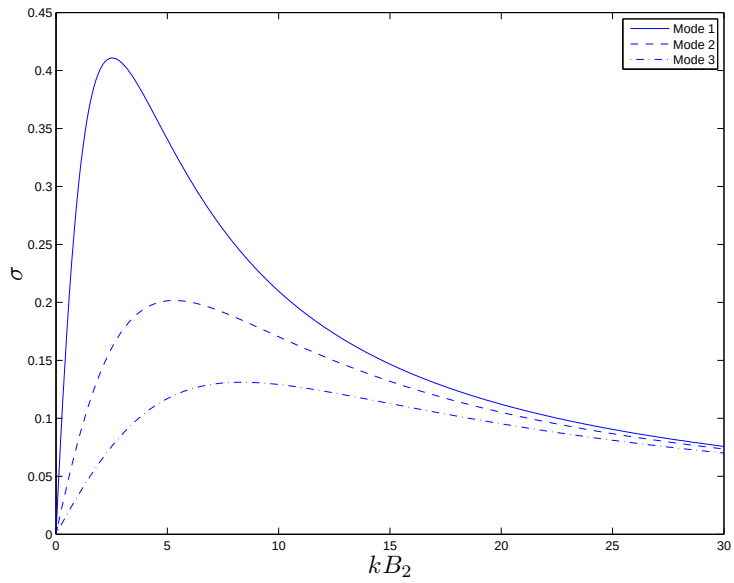

Figure 3.6: The dispersion ratio plotted against kB_2 for the exponential shelf

Figure 3.6 illustrates the fact that each of the shelf modes has a zero group velocity at some intermediate wavenumber. Since this thesis focuses on shelf waves on the Norwegian shelf, it is important to know what wavenumbers that can be expected in this particular region. To discuss the wavelengths, it is necessary to take the generation of the shelf waves into account. The details of the generation of shelf waves are beyond the scope

of this thesis, but has been studied in detail by Gill and Schumann (1974) and Adams and Buchwald (1969). Considering only the wavenumbers, it is sufficient to know that the shelf waves are created by atmospheric disturbances, and that typically have wavelengths larger than 1000 km (see for instance the extensive review by Mysak (1980b)). It can be seen from figure 3.6 on the page before such waves would always have positive (northwards) group velocity in our model of the Norwegian shelf. However, being situated so far to the north, it is possible that polar low-pressure systems, with much smaller extension, passing across or along the shelf may generate shelf waves. For shelf waves generated by Polar lows, the wavelength λ will be of the order 100 km $-$ 1000 km. For the exponential shelf considered here, with $B_2 \approx 155$ km we then have $kB_2 = 2\pi B_2/\lambda$ of the order $1 - 9.7$, with the lower values corresponding to the longer waves. Considering the lowest mode, we see from figure 3.6 on the preceding page that for this range of wavelengths the group velocity may both be positive and negative.

3.2 The interior shelf

From figure 2.1 on page 4 we see that the continental shelf of Norway follows the western coast from Stad and northwards. However, northwest of Lofoten, the depth contours suddenly depart from the direction of the coast, and continue into the Barentz Sea towards Bear Island and Svalbard. Even though the escarpment itself continues as an interior shelf, the waves studied in the previous section can no longer exist in the same form because there is no longer a coastal boundary. A question that immediately arises is then whether disturbances created over the continental shelf may continue to propagate as shelf waves into the Barentz Sea region. Following Buchwald and Adams (1968), the interior shelf will be modelled in a similar way to that used in the previous section. The same exponential form of the shelf will be applied, but with infinite flat ocean beds on each side. For simplicity the width of the shelf and the depths, H_1 and H_2 will be the same as before, but to avoid confusion the width will now be denoted by B_3. As seen in figure 2.1 on page 4, this fits reasonably well with the actual bottom topography. The interior shelf model is shown in figure 3.7.

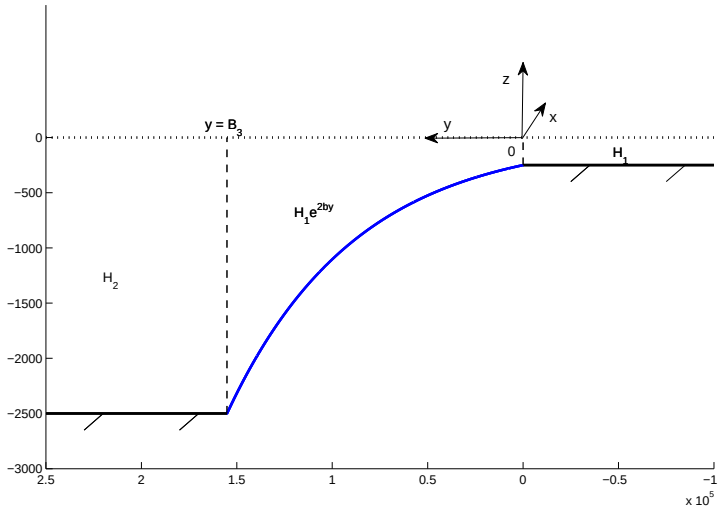

Figure 3.7: Interior shelf model, the x-axis pointing northwards.

The depth is then given by

$$H(y) = \begin{cases} H_1, & y \leq 0 \\ H_1 e^{2by}, & 0 \leq y \leq B_3 \\ H_2, & y \geq B_3, \end{cases} \tag{3.2.1}$$

where

$$H_2 = H_1 e^{2bB_3}, \tag{3.2.2}$$

assuring continuity of H at $y = B_3$.
Assuming wavesolutions of the form

$$\psi = H^{\frac{1}{2}}\phi(y)e^{i(kx-\omega t)}, \tag{3.2.3}$$

as in (3.1.19), and inserting into (2.2.5) on page 9, we get the same differential equation for ϕ as we did for the exponential shelf

$$\frac{d^2\phi}{dy^2} + \left[\frac{d}{dy}\left(\frac{1}{2H}\frac{dH}{dy}\right) - \left(\frac{1}{2H}\frac{dH}{dy}\right)^2 - k^2 + \frac{fk}{\omega}\frac{1}{H}\frac{dH}{dy}\right]\phi = 0 \tag{3.2.4}$$

This equation may be solved in each of the three areas in (3.2.1). Let areas (1), (2) and (3) be $y \leq 0$, $0 \leq y \leq B_3$ and $y \geq B_3$, respectively. By insertion from (3.2.1) into (3.2.4) we then get for area (1) that

$$\frac{d^2\phi_1}{dy^2} - k^2\phi_1 = 0 \tag{3.2.5}$$

A solution to (3.2.5) that stays finite as $y \to -\infty$ is

$$\phi_1 = A_1 e^{ky}, \tag{3.2.6}$$

where A_1 is a constant.
For area (2), insertion from (3.2.1) into (3.2.4) gives the differential equation

$$\frac{d^2\phi_2}{dy^2} + \left[-b^2 - k^2 + \frac{2fkb}{\omega}\right]\phi_2 = 0, \tag{3.2.7}$$

which has the general solution

$$\phi_2 = A_2\sin(ly) + A_3\cos(ly), \tag{3.2.8}$$

As in (3.1.32), l must be given by

$$l = \sqrt{-b^2 - k^2 + \frac{2fkb}{\omega}} \tag{3.2.9}$$

For area (3) the differential equation becomes like in area (1)

$$\frac{d^2\phi_3}{dy^2} - k^2\phi_3 = 0, \tag{3.2.10}$$

but in this case, to keep the solution finite as $y \to \infty$, the general solution becomes

$$\phi_3 = A_4 e^{-ky} \tag{3.2.11}$$

Inserting the solutions for ϕ from (3.2.6), (3.2.8) and (3.2.11) into (3.2.3), using the shelf profile from (3.2.1), we find for the interior shelf waves that

$$\psi = \begin{cases} A_1 e^{ky} H_1^{\frac{1}{2}} e^{i(kx-\omega t)}, & y < 0 \\ \left(A_2 \sin(ly) + A_3 \cos(ly)\right) H_1^{\frac{1}{2}} e^{by} e^{i(kx-\omega t)}, & 0 < y < B_3 \\ A_4 e^{-ky} H_1^{\frac{1}{2}} e^{bB_3} e^{i(kx-\omega t)}, & y > B_3 \end{cases} \tag{3.2.12}$$

In chapter 3.1.2 we found that in the case of an exponential shelf, ψ and $\partial\psi/\partial y$ had to be continuous at $y = B_2$. Here, for the interior shelf shown in figure 3.7 on page 25, this has to be satisfied at both $y = 0$ and $y = B_3$. Using (3.2.12) the conditions for continuity of ψ and $\partial\psi/\partial y$ at $y = 0$ and $y = B_3$ are, as was found by Buchwald and Adams (1968), that

$$A_1 - A_3 = 0, \tag{3.2.13}$$

$$kA_1 - lA_2 - bA_3 = 0, \tag{3.2.14}$$

$$sA_2 + cA_3 - A_4 e^{-kB_3} = 0, \tag{3.2.15}$$

$$(bs + lc)A_2 + (bc - ls)A_3 + kA_4 e^{-kB_3} = 0, \tag{3.2.16}$$

where $s = \sin(lB_3)$ and $c = \cos(lB_3)$. The equations (3.2.13) - (3.2.16) can be combined to eliminate the constants.
Using (3.2.13) in (3.2.14) gives

$$A_2 = \frac{k-b}{l} A_3, \tag{3.2.17}$$

which, together with (3.2.13), inserted into (3.2.15) give

$$A_4 = e^{kB_3} \left(\frac{s(k-b)}{l} + c \right) A_3 \tag{3.2.18}$$

Inserting (3.2.17) and (3.2.18) into (3.2.16), we get that

$$\left((bs + lc)\frac{k-b}{l} + (bc - ls) + k\left(\frac{s(k-b)}{l} + c \right) \right) A_3 = 0 \tag{3.2.19}$$

The condition that equations (3.2.13) - (3.2.16) have a nontrivial solution is then that

$$(bs + lc)\frac{k-b}{l} + (bc - ls) + k\left(\frac{s(k-b)}{l} + c \right) = 0 \tag{3.2.20}$$

$$\Leftrightarrow \quad \tan(lB_3) = \frac{2kl}{l^2 + b^2 - k^2} \tag{3.2.21}$$

Using (3.2.13), (3.2.17) and (3.2.18) in (3.2.12), with $A_3 = D_3$ the equation for ψ becomes

$$\psi = \begin{cases} D_3 e^{ky} H_1^{\frac{1}{2}} e^{i(kx-\omega t)}, & y < 0 \\ D_3 \left(\frac{k-b}{l} \sin(ly) + \cos(ly) \right) H_1^{\frac{1}{2}} e^{by} e^{i(kx-\omega t)}, & 0 < y < B_3 \\ D_3 \left(\frac{s(k-b)}{l} + c \right) H_1^{\frac{1}{2}} e^{(k+b)B_3} e^{-ky} e^{i(kx-\omega t)}, & y > B_3 \end{cases} \tag{3.2.22}$$

The dispersion relation $\omega(k)$ is, as in chapter 3.1.2, given implicitly by two equations for ω, k and l. The equations are (3.2.9) and (3.2.21). Rearranging (3.2.9), we have, as in (3.1.40), that

$$\frac{\omega}{f} = \frac{2kb}{k^2 + l^2 + b^2} \tag{3.2.23}$$

In the same way as was done in chapter 3.1.2, (3.2.21) can be solved for l graphically. (3.2.21) is equivalent to

$$\tan(\hat{l}) = \frac{2\hat{k}\hat{l}}{\hat{l}^2 + \hat{b}^2 - \hat{k}^2} \quad , \tag{3.2.24}$$

where $\hat{l} = lB_3$, $\hat{k} = kB_3$ and $\hat{b} = bB_3$.
While the left hand side of (3.2.24) is the same as it is in (3.1.44), the right hand side is not a straight line anymore. Now, the right hand side has a singularity at $\hat{k}^2 = \hat{l}^2 + \hat{b}^2$. Let $S_{\hat{k}}$ denote the graph of the right hand side of (3.2.24). Consider the case $\hat{k}^2 = \hat{b}^2 + \delta^2 > \hat{b}^2$, which can be seen in figure 3.8 on the next page. From this figure we see that $S_{\hat{k}}$ has an asymptote at $\hat{l} = \delta$. It is also obvious from figure 3.8 that for $\hat{k} \geq \hat{b}$, there is only one solution of (3.2.24) in each interval $(n-1)\pi < \hat{l} \leq n\pi$, where $n = 1, 2, 3$, etc. Also observe that for $\hat{k} = \hat{b}$, i.e. $\delta = 0$, all the intersections are at $\hat{l} < (n - 1/2)\pi$.
Now consider the case when $\hat{k} < \hat{b}$, which has been sketched in figure 3.9 on the following page. Combining the two cases, it may be seen that for $n \geq 2$, $\hat{l}_n(\hat{k})$ varies monotonously from $(n-1)\pi$ to $n\pi$ as $\hat{k}$ varies from 0 to ∞, as pointed out by Buchwald and Adams (1968). Accordingly, we may use the argument following (3.1.48) for the second and higher modes, to show that the shapes of the dispersion curves are actually much the same as was the case with the exponential shelf with a coastal boundary.

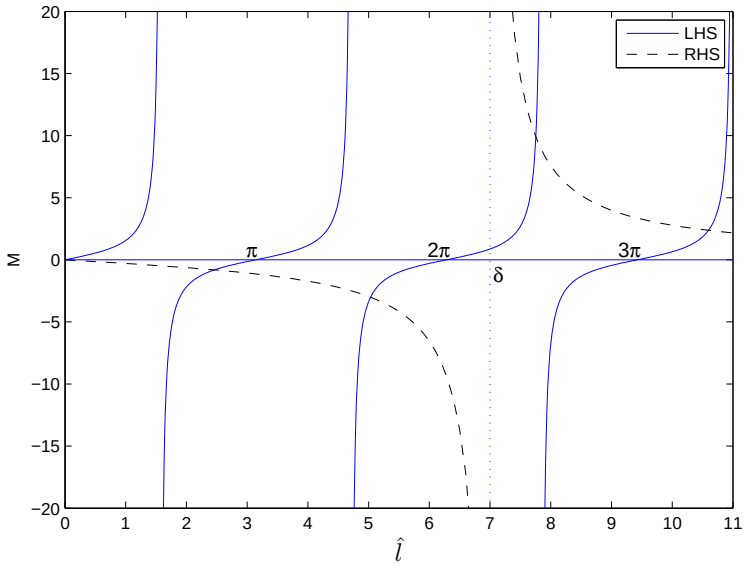

Figure 3.8: Graphical solutions of 3.2.24 for $\hat{k} > \hat{b}$. The left hand side is denoted by LHS, and the right hand side by RHS.

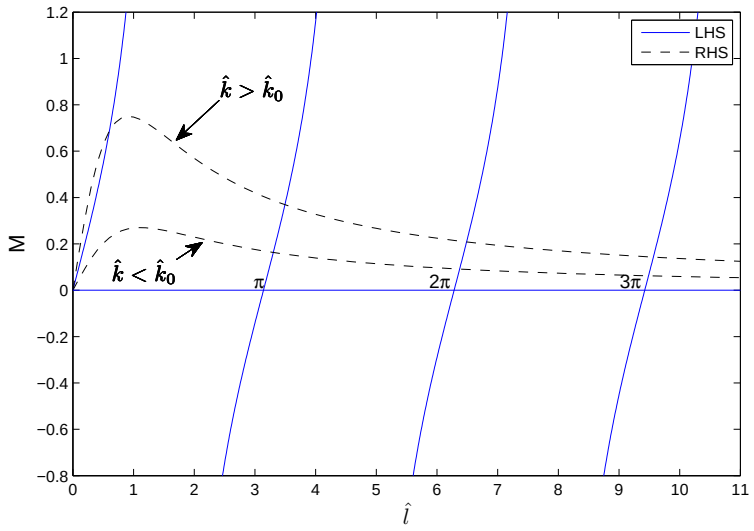

Figure 3.9: Graphical solutions of 3.2.24 for $\hat{k} < \hat{b}$. The left hand side is denoted by LHS, and the right hand side by RHS.

The first mode, however, shows a different behaviour, and the details are explained in Appendix A. The dispersion ratio, σ, for the first three modes of the interior shelf waves is plotted in figure 3.10.

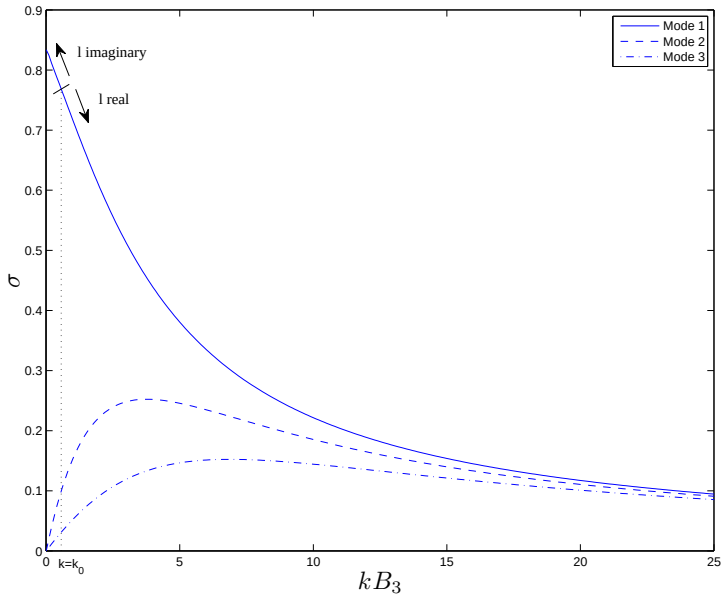

Figure 3.10: The dispersion ratio plotted against kB_3 for the interior shelf

The dispersion diagram illustrates that the group velocity is always in the negative x-direction for the first mode. Since the energy always travels in the direction of the group velocity, this means that in this model, a disturbance created over the continental shelf, could never be communicated to the interior shelf region as a first mode shelf wave. While we have found, in this section, that shelf waves may propagate along a shelf even without a coastal boundary present, it is important to stress that for the wind to generate such waves, the coastal boundary is important (Gill and Schumann, 1974). This implies that waves that propagate along the interior shelf are generated elsewhere. While we will not investigate this any further, it is interesting to note that from figure 2.1 on page 4, it can be seen that a possible generation area for shelf waves over the interior shelf could be the shelf of Svalbard (in the case of short waves with c_g southwards).

3.3 Summary and interpretations

In this chapter we have worked with linear theory to describe the propagation of shelf waves along a straight shelf, considering two different shelf profiles. The dimensions of the shelves were chosen to fit the dimensions of the Norwegian continental shelf, and the interior shelf north of Norway. The two specific ways of representing the bottom topography altered the vorticity equation, and gave rise to waves with different characteristics.

We started out with the simplest possible way of representing the shelf topography, by a single-step shelf. Using this depth profile we found that only one shelf wave mode can exist, and from the dispersion curve we found that the group and phase velocity are always in the same direction, following the shelf with the shallower water to the right.

By applying the exponential shelf profile, the solution to the vorticity equation gave rise to several wave modes. In this case we found that each shelf wave mode is non-dispersive at low wave numbers, and that for some intermediate wave number, the group velocity is zero. Since the group velocity can be both positive and negative, these waves, depending on the wavelength, could communicate disturbances in either direction of the shelf. From the dispersion diagram we saw that the group velocity was only negative in the case of relatively short waves. Wavelengths of this scale are expected to occur, assuming small polar low-pressure systems can generate shelf waves along the western coast of Norway.

Finally, we investigated the propagation of shelf waves along the interior shelf north of Norway. Using the exponential profile also here, the only difference from the continental shelf case was that there was no coastal boundary. This somewhat altered the dispersion relation, especially for the first wave mode, for which l becomes complex for wavenumbers smaller than k_0. This means that the variation over the shelf changes from being trigonometric to hyperbolic in nature. We found that the frequency was monotonically decreasing with k, even through $k = k_0$ (see appendix A), which means that the group velocity is always in the opposite direction of the phase velocity for the first mode.

From the stream function solutions for all the three different shelf profiles it can be seen that the shelf wave amplitudes are exponentially trapped against the shelf. All the results in this chapter are based shallow water theory, assuming a homogeneous ocean, and motion on an f-plane. Furthermore, neglecting all forcing terms in the momentum equation (see chapter 2), this section only deals with freely propagating waves.

Chapter 4

Nonlinear theory for shelf waves

In the previous chapters, theory for the propagation of continental shelf waves along the western coast of Norway has been established. To solve the equations the coast was assumed straight, and two different models for the bottom topography were considered. The propagation of shelf waves along the interior shelf north of Norway has also been investigated, and it was found that in any of the cases considered, the wave amplitude is exponentially trapped against the shelf. This chapter deals with nonlinear theory for this type of waves. First we will work with classical Stokes theory, and then we will include the effect of friction in our analysis, working with the equations of motion to second order accuracy in wave amplitude. The final goal is then to estimate the total drift induced by the shelf waves, and to see how it varies over the shelf, depending on the choice of bottom topography.

The velocities
When finding the dispersion relations in chapter 3, only the stream function was considered, and the velocities themselves were irrelevant. To find the drift the velocities are needed. Assuming that the real parts of the velocities are the physical parts, and using (2.2.4) on page 9, we then find that

$$\begin{aligned} u &= Re\left\{-\frac{1}{H}\frac{\partial\psi}{\partial y}\right\} \\ v &= Re\left\{\frac{1}{H}\frac{\partial\psi}{\partial x}\right\} \end{aligned} \tag{4.0.1}$$

In the equations for the stream functions in the three different models that have been treated, there are still three constants, namely D_1, D_2 and D_3, that remain to be determined. In order to find correct values for these constants, one would have to use models or empirical data from

measurements to find the velocity amplitudes, and then relate these to D_1, D_2 and D_3 through (4.0.1). Since we from now on will deal with the velocities, the following velocity amplitudes are introduced:

$$u_1 \equiv \frac{D_1 k}{H_1}, \qquad u_2 \equiv \frac{D_2 k}{\sqrt{H_1}}, \qquad u_3 \equiv \frac{D_3 k}{\sqrt{H_1}}, \tag{4.0.2}$$

with dimensions ms^{-1}. Using the velocity amplitudes from (4.0.2) it will be easier to keep track of the dimensions in the further calculations of this chapter.
To find appropriate values of the amplitudes u_1, u_2 and u_3 without considering the generation of the shelf waves, is not straight forward. As pointed out by Gill and Schumann (1974), continental shelf waves have been observed by direct current measurements, typically of the order $0.1\ \mathrm{ms}^{-1}$. On the other hand, numerical experiments by Martinsen et al. (1979) show mean current velocities of up to $1.6\ \mathrm{ms}^{-1}$ northwest of Lofoten. Although these high current velocities may be caused partly by errors introduced by the numerical representation of the narrow shelf zone (Martinsen et al., 1979), the result may indicate that current velocities induced by shelf waves may be more than $0.1\ \mathrm{ms}^{-1}$ over the Norwegian Shelf. Considering shelf waves off the western coast of Australia and a square wave forcing with amplitude $0.1\ \mathrm{Nm}^{-2}$, Gill and Schumann (1974) found theoretical maximum values of $0.22\ \mathrm{ms}^{-1}$, $0.17\ \mathrm{ms}^{-1}$ and $0.09\ \mathrm{ms}^{-1}$ for mode 1, 2 and 3, respectively.
Here, when considering examples of the drift over the exponential shelf induced by the first wave mode, we will assume velocities at the coast of $u(y = 0) = 0.5\ \mathrm{ms}^{-1}$.

4.1 The Stokes drift

It was first discovered by Stokes (1847) that wave motion can induce a slow net drift, later called the Stokes drift, of the individual fluid particles in the wave propagation direction. In this section a general expression for the Stokes drift will be derived, following the classical work by Longuet-Higgins (1953), and the result will be applied to the shelf waves described in the previous chapter. To obtain the net particle motion, the Lagrangian velocity, which is the velocity of an individual fluid particle, will be considered. Let $\vec{v}_L(\vec{r}_0, t)$ be the velocity of a fluid particle whose position at time $t = t_0$ is $\vec{r}_0 = (x_0, y_0, z_0)$. After some time, the particle will have moved to a new position

$$\vec{r}_L = \vec{r}_0 + D\vec{r}, \tag{4.1.1}$$

where

$$D\vec{r} = \int_{t_0}^{t} \vec{v}_L(\vec{r}_0, t')dt' \tag{4.1.2}$$

In the Eulerian specification, the fluid velocity at time t is $\vec{v}(x,y,z,t) = \vec{v}(\vec{r}_L,t)$. Using (4.1.1) we then obtain that

$$\vec{v}_L(\vec{r}_0,t) = \vec{v}(\vec{r}_0 + D\vec{r},t) \tag{4.1.3}$$

Assuming that the distance $D\vec{r} = \vec{r}_L - \vec{r}_0$, travelled in the time interval $t - t_0$ is small, the two first terms of a Taylor series expansion give us the relation

$$\begin{aligned} \vec{v}(\vec{r}_0,t) =& \vec{v}(\vec{r}_0,t) + \frac{\partial \vec{v}}{\partial x_0}Dx + \frac{\partial \vec{v}}{\partial y_0}Dy + \frac{\partial \vec{v}}{\partial z_0}Dz \\ =& \vec{v}(\vec{r}_0,t) + D\vec{r}\cdot\nabla_L\vec{v}, \end{aligned} \tag{4.1.4}$$

where $\nabla_L \equiv \vec{i}\frac{\partial}{\partial x_0} + \vec{j}\frac{\partial}{\partial y_0} + \vec{k}\frac{\partial}{\partial z_0}$. Using (4.1.2) in (4.1.4) we can now write

$$\vec{v}_L(\vec{r}_0,t) = \vec{v}(\vec{r}_0,t) + \left(\int_{t_0}^{t} \vec{v}_L(\vec{r}_0,t')dt'\right)\cdot\nabla_L\vec{v}(\vec{r}_0,t) \tag{4.1.5}$$

While the first term on the right hand side of (4.1.5) is the Eulerian velocity $\vec{v}_E$, the second term is the Stokes velocity $\vec{v}_S$, hence we can simply write

$$\vec{v}_L = \vec{v}_E + \vec{v}_S \tag{4.1.6}$$

Now, from (4.1.5), we see that to find the Stokes velocity, we need an expression for the Lagrangian velocity. It has, however, been shown by Longuet-Higgins (1953), that for waves with small wave steepness, the Lagrangian velocity and the Eulerian velocity are equal to first order in wave steepness, so that we can substitute $\vec{v}_L$ by $\vec{v}$ in the integral of (4.1.5). The Stokes velocity is then, to second order in wave steepness, given by

$$\vec{v}_S = \left(\int_{t_0}^{t} \vec{v}(\vec{r}_0,t')dt'\right)\cdot\nabla_L\vec{v}(\vec{r}_0,t) \tag{4.1.7}$$

The wave steepness is given by $kA/2\pi$, or simply

$$\frac{A}{\lambda}, \tag{4.1.8}$$

where λ is the wavelength and A is the amplitude. For the shelf waves considered here, where A must be smaller than the shelf width B and λ is of the size of a low-pressure system, the wave steepness must indeed be small. Averaging the Stokes velocity over a wave period T, we get the Stokes drift

$$\bar{\vec{v}}_S = \frac{1}{T}\int_0^T \vec{v}_S dt, \tag{4.1.9}$$

which constitutes a mean current induced by the waves. From (4.1.6) we see that the Stokes drift is essentially the same as the difference between

the Lagrangian mean and the Eulerian mean velocity. For the shelf waves that will be considered here, the Stokes drift components are

$$\bar{u}_S = \frac{1}{T}\int_0^T \left\{ \left(\int_0^t u dt' \right) \frac{\partial u}{\partial x} + \left(\int_0^t v dt' \right) \frac{\partial u}{\partial y} \right\} dt, \tag{4.1.10}$$

$$\bar{v}_S = \frac{1}{T}\int_0^T \left\{ \left(\int_0^t u dt' \right) \frac{\partial v}{\partial x} + \left(\int_0^t v dt' \right) \frac{\partial v}{\partial y} \right\} dt, \tag{4.1.11}$$

where t_0, since it is arbitrary, has been chosen to be zero.
Recall from chapter 2, that we have applied the rigid lid approximation in our linear analysis, and that the continuity equation then is given by (2.1.23) on page 8. This made it possible to introduce a stream function as in (2.2.4). For all the wave solutions we found in chapter 3, a separation of variables of the form of (2.2.6) was used, and it can then be seen that both of the products inside the outer integral in (4.1.11) are of the form $(...)\sin(2(kx - \omega t))$. Since we average over a wave period, it is then obvious that $\bar{v}_S$ is zero for all the wave solutions in chapter 3.
The Stokes flux, which is the total horizontal mean wave momentum per unit density $(\bar{U}_S)$ can be found by integrating the Stokes velocity (4.1.7) from the bottom to the material surface and then average like in (4.1.9), i.e.

$$\bar{U}_S = \overline{\int_{-H}^{\eta} u_S \, dz} \tag{4.1.12}$$

To second order in wave amplitude, this becomes

$$\bar{U}_S = \int_{-H}^{0} \bar{u}_S \, dz \tag{4.1.13}$$

where $\bar{u}_S$ is the Stokes drift component from (4.1.10). Here, since the Stokes drift component in the direction normal to the phase propagation direction is zero, $\bar{V}_S = 0$.

4.1.1 The step shelf model

For $0 \leq y \leq B_1$, $H = H_1$ and

$$\psi = D_1 \sinh(ky) e^{i(kx - \omega t)}, \tag{4.1.14}$$

which, by using (4.0.1), gives the velocities

$$u = -u_1 \cosh(ky)\cos(kx - \omega t) \tag{4.1.15}$$

$$v = -u_1 \sinh(ky)\sin(kx - \omega t) \tag{4.1.16}$$

Using (4.1.15) and (4.1.16), the Stokes drift given by (4.1.10) can be found for this region. Evaluating all the integrals and derivatives, and after some algebra we find that

$$\bar{u}_S = \frac{u_1^2 k}{2\omega}\cosh(2ky), \qquad 0 \leq y \leq B_1 \tag{4.1.17}$$

The Stokes flux can then be found by inserting (4.1.17) into (4.1.13), which gives

$$\bar{U}_S = \frac{u_1^2 k H_1}{2\omega}\cosh(2ky), \qquad 0 \leq y \leq B_1 \tag{4.1.18}$$

In the deep sea region, where $y > B_1$, we have that $H = H_2$ and

$$\psi = D_1 \sinh(kB_1)e^{-k(y-B_1)}e^{i(kx-\omega t)} \tag{4.1.19}$$

Using (4.0.1) we then find that

$$u = u_1\frac{H_1}{H_2}\sinh(kB_1)e^{-k(y-B_1)}\cos(kx-\omega t), \tag{4.1.20}$$

$$v = -u_1\frac{H_1}{H_2}\sinh(kB_1)e^{-k(y-B_1)}\sin(kx-\omega t). \tag{4.1.21}$$

Inserting these velocities into (4.1.10) this time yields that

$$\bar{u}_S = 0, \qquad y > B_1 \tag{4.1.22}$$

With zero Stokes drift, the Stokes flux is also zero for $y > B_1$. Hence, by integrating (4.1.18) over the shelf region, we can find the total volume flux, $\bar{U}_{ST}$, induced by the Stokes drift over the step-shelf:

$$\bar{U}_{ST} = \frac{u_1^2 k H_1}{2\omega}\int_0^{B_1}\cosh(2ky)\,dy = \frac{u_1^2 H_1}{4\omega}\sinh(2kB_1) \tag{4.1.23}$$

From (4.1.17) and (4.1.22), it is easy to see that the Stokes drift over the step shelf is in the positive x-direction, and increases from the coast to the edge, where $y = B_1$.

4.1.2 The exponential shelf model

For the exponential shelf, in the region $0 \leq y < B_2$, we have that $H = H_1 e^{2by}$ and

$$\psi = D_2 H_1^{\frac{1}{2}} e^{b(y-B_2)}\sin(ly)e^{i(kx-\omega t)}. \tag{4.1.24}$$

By the use of (4.0.1) the velocities then become

$$u = -u_2 e^{-b(y+B_2)}\cdot\left(\frac{b\sin(ly)+l\cos(ly)}{k}\right)\cos(kx-\omega t), \tag{4.1.25}$$

$$v = -u_2 e^{-b(y+B_2)}\sin(ly)\sin(kx-\omega t), \tag{4.1.26}$$

Inserting the velocities (4.1.25) and (4.1.26) into (4.1.10), it can now be found that

$$\bar{u}_S = \frac{u_2^2 k}{2\omega} e^{-2b(y+B_2)} \left[\frac{l^2 \cos(2ly) + bl \sin(2ly)}{k^2} \right], \qquad 0 \leq y < B_2 \quad (4.1.27)$$

Using this in (4.1.13), with $H = H_1 e^{2by}$, the Stokes flux becomes

$$\begin{aligned} \bar{U}_S =& H_1 e^{2by} \cdot \bar{u}_S \\ =& \frac{u_2^2 k H_1}{2\omega} e^{-2bB_2} \left[\frac{l^2 \cos(2ly) + bl \sin(2ly)}{k^2} \right], \qquad 0 \leq y < B_2 \end{aligned} \quad (4.1.28)$$

In the deep ocean, i.e. for $y > B_2$, $H = H_2 = H_1 e^{2bB_2}$ and

$$\psi = D_2 H_1^{\frac{1}{2}} e^{k(B_2 - y)} \sin(lB_2) e^{i(kx - \omega t)} \quad (4.1.29)$$

Using (4.0.1), the velocities then become

$$u = u_2 e^{k(B_2 - y) - 2bB_2} \sin(lB_2) \cos(kx - \omega t) \quad (4.1.30)$$

$$v = -u_2 e^{k(B_2 - y) - 2bB_2} \sin(lB_2) \sin(kx - \omega t), \quad (4.1.31)$$

and with this inserted into (4.1.10) and (4.1.10) we get that

$$\bar{u}_S = \frac{u_2^2 k}{\omega} e^{2k(B_2 - y) - 4bB_2} \sin^2(lB_2), \qquad y > B_2 \quad (4.1.32)$$

The Stokes flux, using (4.1.13) and that $H = H_1 e^{2bB_2}$, simply becomes

$$\bar{U}_S = \frac{u_2^2 k H_1}{\omega} e^{2k(B_2 - y) - 2bB_2} \sin^2(lB_2), \qquad y > B_2 \quad (4.1.33)$$

The total Stokes flux over the exponential shelf can be obtained by integrating (4.1.28) from $y = 0$ to $y = B_2$, (4.1.33) from $y = B_2$ to $y = \infty$ and adding the result:

$$\begin{aligned} \bar{U}_{ST} =& \frac{u_2^2 H_1}{2\omega k} e^{-2bB_2} \int_0^{B_2} \left(l^2 \cos(2ly) + bl \sin(2ly) \right) dy \\ &+ \frac{u_2^2 H_1 k}{\omega} e^{2kB_2 - 2bB_2} \sin^2(lB_2) \int_{B_2}^{\infty} e^{-2ky} dy \end{aligned} \quad (4.1.34)$$

Solving the integrals in (4.1.34), we find that

$$\bar{U}_{ST} = \frac{u_2^2 H_1}{4\omega} e^{-2bB_2} \left[\frac{l \sin(2lB_2) + (k+b)\big(1 - \cos(2lB_2)\big)}{k} \right] \quad (4.1.35)$$

Using equation (4.1.27) and (4.1.32), the distribution of the Stokes drift over the exponential shelf can be plotted. The equations are scaled by the maximum value, occurring at the coast ($y = 0$). To find the total Stokes drift induced by the shelf wave, a superposition of the modes is needed. Here, we will however assume that the first mode is dominating, and therefore only the Stokes drift induced by the first mode is plotted. Choosing wavelengths of 200 km and 800 km, corresponding to $kB_2 = 4.87$ and $kB_2 = 1.22$, respectively, both the cases of positive and negative group velocity are considered (see figure 3.6 on page 23).

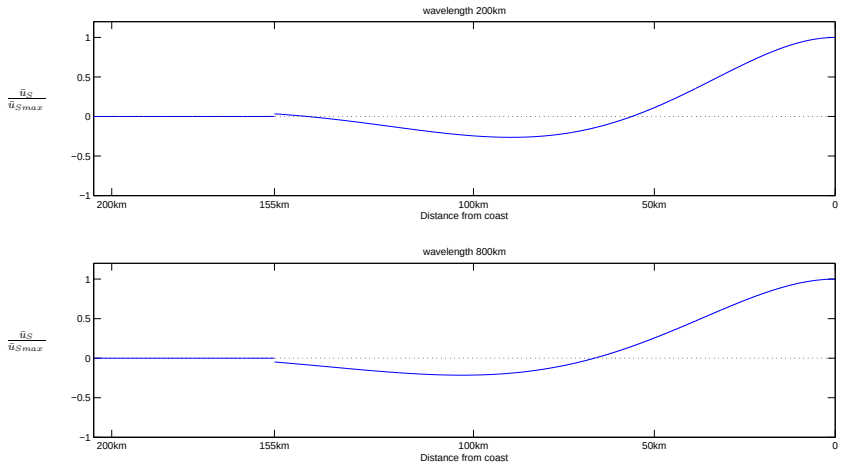

Figure 4.1: The scaled Stokes drift over the exponential shelf, plotted against the distance from the shore

From figure 4.1 we see that both the wave of 200 km and the wave of 800 km induce a Stokes drift that is in the positive x-direction, i.e. northwards, close to the coast, where it is greatest in magnitude. Further offshore, in both cases, the Stokes drift changes direction and reaches a minimum before it decreases in magnitude towards the shelf edge. From the shelf edge and further offshore, the Stokes drift is northwards, very small in magnitude relative to the maximum and decreasing exponentially. This is hard to see from the figure, since the scaled drift becomes so small beyond the shelf edge.

An example of the Stokes drift

As an example of the Stokes drift velocity we will here consider the theoretical magnitude of the Stokes drift at the coast, provided that there are measurements of a wave-induced velocity amplitude at the coast of 0.5 ms^{-1}, as argued in the beginning of this chapter. It will be assumed that this is induced solely by the gravest wavemode. With this observed maximum ve-

locity, (4.1.25) at $y = 0$ can be used to solve for u_2, for a given wavenumber k. For the two wavelength in figure 4.1, it can then be found that approximately

$$|u_2| = 2.84 \text{ ms}^{-1}, \quad k = \frac{2\pi}{200 \text{ km}} \tag{4.1.36}$$

$$|u_2| = 0.82 \text{ ms}^{-1}, \quad k = \frac{2\pi}{800 \text{ km}} \tag{4.1.37}$$

Inserting these values into (4.1.27) for $y = 0$, we find that the Stokes drift at the coast is

$$\bar{u}_S(y = 0) = 8.71 \text{ cm s}^{-1} \quad k = \frac{2\pi}{200 \text{ km}} \tag{4.1.38}$$

$$\bar{u}_S(y = 0) = 2.25 \text{ cm s}^{-1} \quad k = \frac{2\pi}{800 \text{ km}} \tag{4.1.39}$$

4.1.3 The Interior Shelf

In the shallow region East of the shelf (see figure 3.7 on page 25), where $y < 0$ and $H = H_1$, the stream function is given by

$$\psi = D_3 e^{ky} H_1^{\frac{1}{2}} e^{i(kx-\omega t)} \tag{4.1.40}$$

Using (4.0.1), the velocities then become

$$u = -u_3 e^{ky} \cos(kx - \omega t) \tag{4.1.41}$$

$$v = -u_3 e^{ky} \sin(kx - \omega t), \tag{4.1.42}$$

Inserting these velocities into (4.1.10), it can then be found that

$$\bar{u}_S = \frac{u_3^2 k}{\omega} e^{2ky}, \qquad y < 0 \tag{4.1.43}$$

Inserting (4.1.43) into (4.1.13), with $H = H_1$ we find that

$$\bar{U}_S = \frac{u_3^2 k H_1}{\omega} e^{2ky}, \qquad y < 0 \tag{4.1.44}$$

For $0 < y < B_3$, $H = H_1 e^{2by}$ and the stream function is given by

$$\psi = D_3 \left(\frac{k-b}{l} \sin(ly) + \cos(ly) \right) H_1^{\frac{1}{2}} e^{by} e^{i(kx-\omega t)} \tag{4.1.45}$$

Using (4.0.1), the velocities then become

$$\begin{aligned} u =& - u_3 e^{-by} \left[\frac{1}{k} \left(\frac{b(k-b)}{l} - l \right) \sin(ly) + \cos(ly) \right] \\ & \cdot \cos(kx - \omega t), \end{aligned} \tag{4.1.46}$$

$$v = - u_3 e^{-by} \left[\frac{k-b}{l} \sin(ly) + \cos(ly) \right] \sin(kx - \omega t), \tag{4.1.47}$$

Inserting these velocities into (4.1.10), it can then be found that

$$\begin{aligned} \bar{u}_S =& \frac{u_3^2 k}{2\omega} e^{-2by} \left\{ \left[\frac{1}{k} \left(\frac{b(k-b)}{l} - l \right) \sin(ly) + \cos(ly) \right]^2 \right. \\ & \left. - \left(\frac{l^2 + b^2}{k^2} \right) \left[\frac{k-b}{l} \sin(ly) + \cos(ly) \right]^2 \right\}, \qquad 0 < y < B_3 \end{aligned} \tag{4.1.48}$$

The Stokes flux is easily found by inserting (4.1.48) into (4.1.13), with $H = H_1 e^{2by}$, which gives us that

$$\begin{aligned} \bar{U}_S =& \frac{u_3^2 k H_1}{2\omega} \left\{ \left[\frac{1}{k} \left(\frac{b(k-b)}{l} - l \right) \sin(ly) + \cos(ly) \right]^2 \right. \\ & \left. - \left(\frac{l^2 + b^2}{k^2} \right) \left[\frac{k-b}{l} \sin(ly) + \cos(ly) \right]^2 \right\}, \qquad 0 < y < B_3 \end{aligned} \tag{4.1.49}$$

For $y > B_3$, $H = H_1 e^{2bB_3}$ and

$$\psi = D_3 \left(\frac{s(k-b)}{l} + c \right) H_1^{\frac{1}{2}} e^{(k+b)B_3} e^{-ky} e^{i(kx - \omega t)} \tag{4.1.50}$$

Using (4.0.1), the velocities this time become

$$u = u_3 e^{(k-b)B_3} \left(\frac{s(k-b)}{l} + c \right) e^{-ky} \cos(kx - \omega t), \tag{4.1.51}$$

$$v = - u_3 e^{(k-b)B_3} \left(\frac{s(k-b)}{l} + c \right) e^{-ky} \sin(kx - \omega t), \tag{4.1.52}$$

Again by inserting the velocities into (4.1.10), we find that

$$\begin{aligned} \bar{u}_S =& \frac{u_3^2 k}{\omega} e^{2(k-b)B_3} \left(\frac{s(k-b)}{l} + c \right)^2 e^{-2ky} \\ & \cdot \frac{1}{T} \int_0^T (\sin^2(kx - \omega t) + \cos^2(kx - \omega t)) dt \\ =& \frac{u_3^2 k}{\omega} e^{2(k-b)B_3} \left(\frac{s(k-b)}{l} + c \right)^2 e^{-2ky}, \qquad y > B_3 \end{aligned} \tag{4.1.53}$$

Inserting (4.1.53) into (4.1.13), with $H = H_1 e^{2bB_3}$, we find that

$$\bar{U}_S = \frac{u_3^2 k H_1}{\omega} e^{2kB_3} \left(\frac{s(k-b)}{l} + c \right)^2 e^{-2ky}, \qquad y > B_3 \tag{4.1.54}$$

Using the results from (4.1.44), (4.1.49) and (4.1.54), integrating over each region and adding, we find that the total Stokes flux over the interior shelf is given by

$$\begin{aligned} \bar{U}_{ST} =& \frac{u_3^2 k H_1}{\omega} \int_{-\infty}^{0} e^{2ky}\, dy \\ &+ \frac{u_3^2 k H_1}{2\omega} \int_0^{B_3} \left\{ \left[\left(\frac{1}{k} \frac{b(k-b)}{l} - l \right) \sin(ly) + \cos(ly) \right]^2 \right. \\ &\qquad \left. - \left(\frac{l^2 + b^2}{k^2} \right) \left[\frac{k-b}{l} \sin(ly) + \cos(ly) \right]^2 \right\} dy \\ &+ \frac{u_3^2 k H_1}{\omega} e^{2kB_3} \left(\frac{s(k-b)}{l} + c \right)^2 \int_{B_3}^{\infty} e^{-2ky} dy \end{aligned} \tag{4.1.55}$$

After some algebra, and inserting that $s = sin(lB_3)$ and $c = cos(lB_3)$, we find that

$$\begin{aligned} \bar{U}_{ST} =& \frac{u_3^2 H_1}{2\omega} \left[\frac{1}{kl^2} \left\{ \left(3l^2 k + 2b^2 k - b^3 - b(l^2 + k^2) \right) \cos^2(lB_3) \right. \right. \\ &+ l \left(3k^2 - 2bk - l^2 - b^2 \right) \sin(lB_3) \cos(lB_3) \\ &\left. \left. + (b-k) \left(k(b-k) \sin^2(lB_3) + b^2 + l^2 - bk \right) \right\} \right] \end{aligned} \tag{4.1.56}$$

As done for the exponential shelf, the scaled Stokes drift over the interior shelf is plotted for the two wavelengths 200 km and 800 km. In this case, the Stokes drift induced by the second mode is also plotted since the first mode shows a different behaviour than the other modes (see figure 3.10 on page 30).

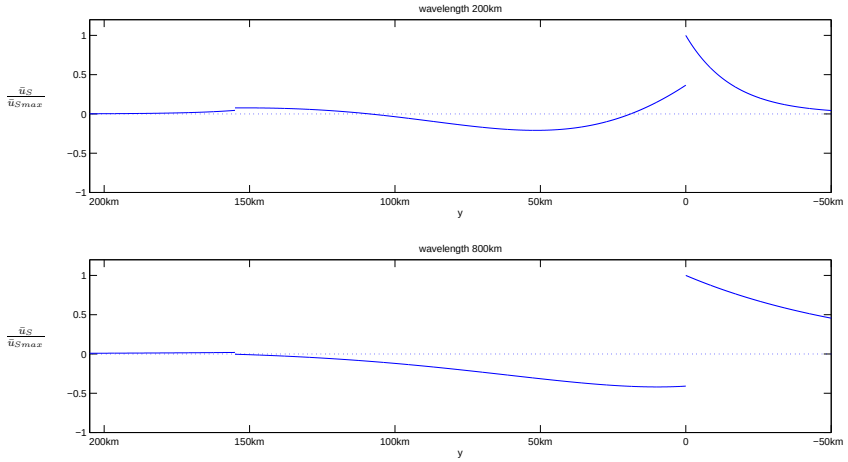

Figure 4.2: The scaled Stokes drift over the interior shelf, mode 1

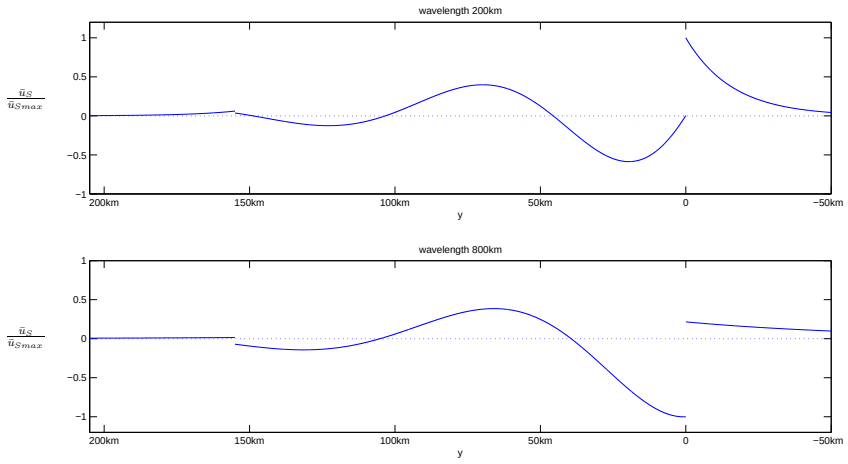

Figure 4.3: The scaled Stokes drift over the interior shelf, mode 2

4.2 The total Lagrangian drift

The Stokes drift, which was described in the previous sub-chapter, is inherent in the wave motion, and essentially is an inviscid phenomenon. In a real ocean, however, the effect of dissipation must be taken into account. Wave amplitude attenuation due to friction transfers momentum to mean Eulerian currents (Longuet-Higgins, 1953), and this type of mean current due to continental shelf waves will be discussed in this section. The mean Eulerian current together with the Stokes drift constitutes the total Lagrangian drift, and the final goal is to make realistic estimates of this drift along the western coast of Norway.

Including friction in the linear equations
To include the effect of dissipation, we will include friction in the original equations, (2.1.10), (2.1.11) and (2.1.23). The friction will be represented in the simplest possible way, i.e. we use the Rayleigh friction, $\vec{F} = -r\vec{v}$, in the momentum equation (2.1.1). Following the argumentation of chapter 2.1, we then end up with the equations

$$\frac{\partial u}{\partial t} - fv = -g\frac{\partial \eta}{\partial x} - ru \tag{4.2.1}$$

$$\frac{\partial v}{\partial t} + fu = -g\frac{\partial \eta}{\partial y} - rv \tag{4.2.2}$$

$$\frac{\partial}{\partial x}(uH) + \frac{\partial}{\partial y}(vH) = 0 \tag{4.2.3}$$

Operating the curl on the vector equation, (4.2.1) and (4.2.2), using (4.2.3) and introducing the stream function (2.2.4) on page 9, the vorticity equation is easily obtained

$$\begin{aligned}\frac{\partial}{\partial t}\left[\frac{\partial}{\partial x}\Big(\frac{1}{H}\frac{\partial \psi}{\partial x}\Big) + \frac{\partial}{\partial y}\Big(\frac{1}{H}\frac{\partial \psi}{\partial y}\Big)\right] - \frac{f}{H^2}\frac{dH}{dy}\frac{\partial \psi}{\partial x} \\ +r\left[\frac{\partial}{\partial x}\Big(\frac{1}{H}\frac{\partial \psi}{\partial x}\Big) + \frac{\partial}{\partial y}\Big(\frac{1}{H}\frac{\partial \psi}{\partial y}\Big)\right] = 0\end{aligned} \tag{4.2.4}$$

As before the solutions will be assumed to be on the form of a complex Fourier component,

$$\psi = H^{\frac{1}{2}}\phi(y)e^{i(\kappa x - \omega t)}, \tag{4.2.5}$$

where $\kappa = k + i\alpha$. Here $k > 0$ is the real wave number, and α is the spatial damping coefficient in the x-direction. Furthermore we shall assume that the wave damping is small over a distance comparable to the wavelength, i.e. $|\alpha| \ll k$, throughout the rest of this analysis. Inserting (4.2.5) into (4.2.4),

we obtain the damped equivalent of (3.1.28)

$$\frac{d^2\phi}{dy^2} + \left[\frac{\partial}{\partial y}\left(\frac{1}{2H}\frac{dH}{dy}\right) - \left(\frac{1}{2H}\frac{dH}{dy}\right)^2 - \kappa^2 + \frac{\kappa f}{\omega + ir}\frac{1}{H}\frac{dH}{dy}\right]\phi = 0 \quad (4.2.6)$$

Now, to further simplify the analysis in this section the attention will be restricted to long waves, i.e. long-shore wavenumbers k for which kB_0 is small. From the discussion of Gill and Schumann (1974), we then know that the boundary conditions become that of no normal flow at the coast and that u vanishes at the edge of the shelf, i.e.

$$\psi = 0 \quad \text{at} \quad y = 0 \quad (4.2.7)$$

$$\frac{\partial \psi}{\partial y} = 0 \quad \text{at} \quad y = B_0 \quad (4.2.8)$$

Inserting $H = H_1 e^{2by}$ into (4.2.6) then yields

$$\frac{d^2\phi}{dy^2} + \left\{-b^2 - \kappa^2 + \frac{2\kappa f b}{\omega + ir}\right\}\phi = 0 \quad (4.2.9)$$

To satisfy the boundary condition (4.2.7), we find that

$$\phi = A_1 \sin(ly), \quad (4.2.10)$$

where l now is given by

$$l = \sqrt{-b^2 - \kappa^2 + \frac{2\kappa f b}{\omega + ir}} \quad (4.2.11)$$

Inserting (4.2.10) into (4.2.5) we then find that

$$\psi = A_1 H_1^{\frac{1}{2}} e^{by} \sin(ly) e^{i(\kappa x - \omega t)}, \quad 0 \le y \le B_0 \quad (4.2.12)$$

Using the boundary condition (4.2.8) in (4.2.12), the transcendental equation becomes

$$\tan(lB_0) = -\frac{l}{b} \quad (4.2.13)$$

It should be noted that (4.2.13) is equal to (3.1.43) on page 20 in the limit $k \to 0$. Now, the dispersion relation is given implicitly by the two equations (4.2.11) and (4.2.13). Rearranging (4.2.11), using that $\kappa = k + i\alpha$, the real part yields that

$$\omega = \frac{2fbk + 2rk\alpha}{l^2 + b^2 + k^2 - \alpha^2}, \quad (4.2.14)$$

while the imaginary part gives us that

$$r = \frac{2fb\alpha - 2\omega k\alpha}{l^2 + b^2 + k^2 - \alpha^2} \quad (4.2.15)$$

Since α is small, terms of $O(\alpha^2)$ will be neglected in the subsequent analysis. From (4.2.15) we see that $r \sim \alpha$, and hence that the term $2rk\alpha$ in the numerator of (4.2.14) is of $O(\alpha^2)$. Hence, to $O(\alpha)$ we have

$$\omega = \frac{2fbk}{l^2 + b^2 + k^2} \tag{4.2.16}$$

$$r = \frac{2fb\alpha - 2\omega k\alpha}{l^2 + b^2 + k^2} \tag{4.2.17}$$

Notice that the dispersion relation with friction to $O(\alpha)$, (4.2.16), is equal to the frictionless dispersion relation, (3.1.40) on page 20.

The velocities

Now we only have velocities for $0 \leq y \leq B_0$, and using (4.2.12) it can easily be found that the real parts of the velocities are given by

$$u = -u_0 e^{-\alpha x - by} \cdot \left(\frac{b\sin(ly) + l\cos(ly)}{k} \right) \cos(kx - \omega t), \tag{4.2.18}$$

$$v = -u_0 e^{-\alpha x - by} \sin(ly) \cdot \left(\frac{k\sin(kx - \omega t) + \alpha\cos(kx - \omega t)}{k} \right), \tag{4.2.19}$$

where

$$u_0 \equiv \frac{A_1 k}{\sqrt{H_1}} \tag{4.2.20}$$

The Stokes flux

Since the Stokes drift is inherent in the periodic wave motion, it is essentially independent on the friction, and it can be argued that it is the Stokes drift calculated without friction in our equations that is correct. In the previous sub-chapter we found that an expression for the longshore Stokes drift in the frictionless case, and by using the velocities given by (4.2.18) and (4.2.19) in (4.1.10), we find that it is similar in the frictional case, except for a weak exponential damping in x:

$$\bar{u}_S = \frac{u_0^2 k}{2\omega} e^{-2\alpha x - 2by} \left[\frac{bl\sin(2ly) + l^2\cos(2ly)}{k^2} \right] \tag{4.2.21}$$

Hence, the Stokes drift is in the wave propagation direction, and any drift normal to this, that is related to the friction will be assumed to be Eulerian. The Stokes flux, using (4.1.13) and that $H = H_1 e^{2by}$, is then given by

$$\bar{U}_S = \frac{u_0^2 k H_1}{2\omega} e^{-2\alpha x} \left[\frac{bl\sin(2ly) + l^2\cos(2ly)}{k^2} \right] \tag{4.2.22}$$

The surface elevation

The x-momentum equation (4.2.1) in terms of ψ is given by

$$\frac{\partial}{\partial t}\left(-\frac{1}{H}\frac{\partial \psi}{\partial y} \right) - f\left(\frac{1}{H}\frac{\partial \psi}{\partial x} \right) = -g\frac{\partial \eta}{\partial x} - r\left(-\frac{1}{H}\frac{\partial \psi}{\partial y} \right) \tag{4.2.23}$$

Assuming that η has the wavelike form of (4.2.5), i.e. that $\eta \sim e^{i(\kappa x-\omega t)}$, then $\partial\eta/\partial x = i\kappa\eta$. Using this it can easily be shown that (4.2.23) is equivalent to

$$gH\eta = f\psi - \frac{\omega + ir}{\kappa}\frac{\partial\psi}{\partial y} \tag{4.2.24}$$

Assuming that the real part represents the physical solution, using that $H = H_1 e^{2by}$, (4.2.12) and that $r \sim \alpha$, solving (4.2.24) for η we find that to $O(\alpha)$

$$\begin{aligned}\eta =& \frac{u_0}{gk}e^{-\alpha x-by}\cdot\left\{\Big[f\sin(ly) - \frac{\omega}{k}\big(b\sin(ly)+l\cos(ly)\big)\Big]\cos(kx-\omega t)\right.\\ &\left. - \frac{\omega\alpha - rk}{k^2}\big(b\sin(ly)+l\cos(ly)\big)\sin(kx-\omega t)\right\}\end{aligned} \tag{4.2.25}$$

The mean Eulerian volume flux

Applying the Boussinesq approximation, integrating the momentum equation (2.1.1) vertically between the material surfaces at the bottom and at the surface, as done by Weber (2009), it can be found for the horizontal fluxes that

$$\begin{aligned}\frac{\partial U_L}{\partial t} - fV_L =& -\frac{1}{\rho_r}\int_{-H}^{\eta}\left(\frac{\partial p}{\partial x}\right)dz + \int_{-H}^{\eta}F^{(x)}dz - \frac{\partial}{\partial x}\int_{-H}^{\eta}u^2\,dz\\ &- \frac{\partial}{\partial y}\int_{-H}^{\eta}uv\,dz,\\ \frac{\partial V_L}{\partial t} + fU_L =& -\frac{1}{\rho_r}\int_{-H}^{\eta}\left(\frac{\partial p}{\partial y}\right)dz + \int_{-H}^{\eta}F^{(y)}dz - \frac{\partial}{\partial x}\int_{-H}^{\eta}uv\,dz\\ &- \frac{\partial}{\partial y}\int_{-H}^{\eta}v^2\,dz,\end{aligned} \tag{4.2.26}$$

where ρ_r is a constant reference density and

$$U_L = \int_{-H}^{\eta}u\,dz \quad and \quad V_L = \int_{-H}^{\eta}v\,dz, \tag{4.2.27}$$

are the Lagrangian volume fluxes. The vertically integrated continuity equation (2.1.8) is then given by

$$\frac{\partial\eta}{\partial t} + \frac{\partial U_L}{\partial x} + \frac{\partial V_L}{\partial y} = 0 \tag{4.2.28}$$

To simplify (4.2.26) it will be assumed that the pressure distribution is hydrostatic, and the horizontal friction force components will be expressed in terms of the horizontal frictional shear stresses $\tau^{(x)}$ and $\tau^{(y)}$, i.e.

$$F^{(x)} = \frac{\partial}{\partial z}\left(\frac{\tau^{(x)}}{\rho_r}\right), \quad F^{(y)} = \frac{\partial}{\partial z}\left(\frac{\tau^{(y)}}{\rho_r}\right) \tag{4.2.29}$$

Furthermore, we will assume that there is no forcing from the wind or the pressure at the surface. Averaging over a wave period, like in (4.1.9), equation (4.2.26) then becomes, to second order in wave amplitude

$$\begin{aligned}\frac{\partial \bar{U}_L}{\partial t} - f\bar{V}_L + gH\frac{\partial \bar{\eta}}{\partial x} + \frac{\bar{\tau}_B^{(x)}}{\rho_r} =& -g\frac{1}{2}\frac{\partial}{\partial x}(\overline{\eta^2}) - \frac{\partial}{\partial x}\left(\int_{-H}^{0}(\overline{u^2})dz\right) \\ & - \frac{\partial}{\partial y}\left(\int_{-H}^{0}(\overline{uv})dz\right) \\ \frac{\partial \bar{V}_L}{\partial t} + f\bar{U}_L + gH\frac{\partial \bar{\eta}}{\partial y} + \frac{\bar{\tau}_B^{(y)}}{\rho_r} =& -g\frac{1}{2}\frac{\partial}{\partial y}(\overline{\eta^2}) - \frac{\partial}{\partial x}\left(\int_{-H}^{0}(\overline{uv})dz\right) \\ & - \frac{\partial}{\partial y}\left(\int_{-H}^{0}(\overline{v^2})dz\right)\end{aligned} \tag{4.2.30}$$

where τ_B is the bottom drag. Since all the terms on the right hand sides of (4.2.30) arise from the periodic wave motion and act on the mean flow, they can be referred to as wave-forcing terms (Weber, 2009). To second order in wave amplitude, all these terms can be completely determined by linear wave theory. Integrating (4.1.6) between the bottom and the free surface, and then average, we also find that

$$\begin{aligned}\bar{U}_L =& \bar{U}_E + \bar{U}_S \\ \bar{V}_L =& \bar{V}_E + \bar{V}_S\end{aligned} \tag{4.2.31}$$

To further simplify (4.2.30), the bottom drag will be assumed to be linear in the Eulerian fluxes, i.e.

$$\bar{\tau}_B^{(x)} = \rho_r K\bar{U}_E, \quad \bar{\tau}_B^{(y)} = \rho_r K\bar{V}_E \tag{4.2.32}$$

Accordingly, K is a constant bottom friction coefficient. While it is generally different from the friction coefficient r in (4.2.1) it will be taken to be of the same order of magnitude. With steady mean flow and averaging over a wave period, the integrated continuity equation (4.2.28) becomes

$$\frac{\partial \bar{U}_L}{\partial x} + \frac{\partial \bar{V}_L}{\partial y} = 0, \tag{4.2.33}$$

or, by using (4.2.31) and that $\bar{V}_S = 0$

$$\frac{\partial \bar{U}_E}{\partial x} + \frac{\partial \bar{U}_S}{\partial x} = -\frac{\partial \bar{V}_E}{\partial y} \tag{4.2.34}$$

From (4.2.22) it is easily seen that $\partial \bar{U}_S/\partial x \sim \alpha$ is small, and hence, from (4.2.34), we must have that

$$\frac{\partial \bar{U}_E}{\partial x} \sim \frac{\partial \bar{V}_E}{\partial y} \tag{4.2.35}$$

Expecting $\bar{U}_E$ and $\bar{V}_E$ to have the same form as $\bar{U}_S$, this becomes

$$\alpha \bar{U}_E \sim l \bar{V}_E, \quad or \quad \left| \frac{\bar{V}_E}{\bar{U}_E} \right| \sim \frac{\alpha}{l} \tag{4.2.36}$$

For long waves, $l > k$ and since $\alpha/k \ll 1$, this means that $\bar{V}_E$ must be much smaller than $\bar{U}_E$. Thus, when inserting (4.2.32) into (4.2.30), when considering steady flow, the term $K\bar{V}_E$ will be neglected. Since u and v, given by (4.2.18) and (4.2.19) respectively, are independent of z, the integrals in (4.2.30) are easily evaluated. Furthermore, considering steady mean flow, and using (4.2.32) and that $H = H(y)$, (4.2.30) gives the two equations

$$\begin{aligned} -f\bar{V}_L + K\bar{U}_E + gH\frac{\partial \bar{\eta}}{\partial x} = &- g\frac{1}{2}\frac{\partial}{\partial x}(\overline{\eta^2}) - 2H\Big(\overline{u\frac{\partial u}{\partial x}}\Big) - \frac{dH}{dy}\overline{uv} \\ &- H\frac{\partial}{\partial y}(\overline{uv}), \end{aligned} \tag{4.2.37}$$

$$\begin{aligned} f\bar{U}_L + gH\frac{\partial \bar{\eta}}{\partial y} = &- g\frac{1}{2}\frac{\partial}{\partial y}(\overline{\eta^2}) - H\frac{\partial}{\partial x}(\overline{uv}) - \frac{dH}{dy}\overline{v^2} \\ &- 2H\Big(\overline{v\frac{\partial v}{\partial y}}\Big) \end{aligned} \tag{4.2.38}$$

Using the equations (4.2.37), (4.2.38) and (4.2.33) we can solve for $\bar{U}_E$, $\bar{V}_E$ and $\bar{\eta}$. Operating the curl on the equations for the Lagrangian volume transport and by using (4.2.33), we find that

$$\begin{aligned} gH'\frac{\partial \bar{\eta}}{\partial x} = &- K\frac{\partial \bar{U}_E}{\partial y} - 2H'\Big(\overline{u\frac{\partial u}{\partial x}}\Big) - 2H\frac{\partial}{\partial y}\Big(\overline{u\frac{\partial u}{\partial x}}\Big) - H''\overline{uv} \\ &- 2H'\frac{\partial}{\partial y}(\overline{uv}) - H\frac{\partial^2}{\partial y^2}(\overline{uv}) + H\frac{\partial^2}{\partial x^2}(\overline{uv}) \\ &+ H'\frac{\partial}{\partial x}(\overline{v^2}) + 2H\frac{\partial}{\partial x}(\overline{v\frac{\partial v}{\partial y}}), \end{aligned} \tag{4.2.39}$$

where $H' = dH/dy$. From (4.2.18) and (4.2.19) it is easy to see that some of the terms in (4.2.39) are of order α^2 or higher, and they will be neglected. Since we consider an exponential shelf profile, where $H = H_1 e^{2by}$, we can use in (4.2.39) that $H' = 2bH$, and hence

$$\begin{aligned} gH\frac{\partial \bar{\eta}}{\partial x} = &- \frac{K}{2b}\frac{\partial \bar{U}_E}{\partial y} - 2H\Big(\overline{u\frac{\partial u}{\partial x}}\Big) - \frac{H}{b}\frac{\partial}{\partial y}\Big(\overline{u\frac{\partial u}{\partial x}}\Big) - H'\overline{uv} \\ &- 2H\frac{\partial}{\partial y}(\overline{uv}) - \frac{H}{2b}\frac{\partial^2}{\partial y^2}(\overline{uv}) + \frac{H}{b}\frac{\partial}{\partial x}(\overline{v\frac{\partial v}{\partial y}}), \end{aligned} \tag{4.2.40}$$

Since $\bar{V}_S = 0$, we have that $\bar{V}_L = \bar{V}_E$, and inserting (4.2.40) into (4.2.37) and rearranging, we find that

$$\begin{aligned}\frac{2fb}{K}\bar{V}_E + \frac{\partial \bar{U}_E}{\partial y} - 2b\bar{U}_E = &-\frac{2H}{K}\frac{\partial}{\partial y}\Big(\overline{u\frac{\partial u}{\partial x}}\Big) - \frac{2bH}{K}\frac{\partial}{\partial y}(\overline{uv}) \\ &-\frac{H}{K}\frac{\partial^2}{\partial y^2}(\overline{uv}) + \frac{2H}{K}\frac{\partial}{\partial x}(\overline{v\frac{\partial v}{\partial y}}) + \frac{bg}{K}\frac{\partial}{\partial x}(\overline{\eta^2})\end{aligned} \tag{4.2.41}$$

To simplify (4.2.41), the last term will be neglected, and to see under which condition this is appropriate, it can be compared in size with any of the other terms, which are all of comparable size. Using (4.2.18), (4.2.25) and the dispersion relation (4.2.16) it can easily be found that to $O(\alpha)$

$$\begin{aligned}\frac{2H}{K}\frac{\partial}{\partial y}\Big(\overline{u\frac{\partial u}{\partial x}}\Big) = &\frac{2u_0\alpha H_1}{K}\frac{b^2+l^2}{k^2}\, e^{-2\alpha x} \\ &\cdot\Big[\sin(ly)\,(b\sin(ly) + l\cos(ly))\Big],\end{aligned} \tag{4.2.42}$$

$$\begin{aligned}\frac{bg}{K}\frac{\partial}{\partial x}(\overline{\eta^2}) = &\frac{u_0^2 b}{gk^2}\frac{\alpha}{K}\, e^{-2\alpha x - 2by}\left(\frac{2fb}{l^2+b^2+k^2}\right)^2 \\ &\cdot\left[\left(\frac{l^2+b^2+k^2}{2b}\right)\sin(ly) - b\sin(ly) - l\cos(ly)\right]^2,\end{aligned} \tag{4.2.43}$$

Considering order of magnitude, it can be seen from equation (3.1.46) and figure 3.5 on page 21, that $l \sim b \sim 1/B_0$. This holds especially well for the first mode, but since this is assumed to be the dominating mode, it will be considered to be generally true. For long waves we also have that $k^2 \ll l^2, b^2$, and from (4.2.42) and (4.2.43) it can then be seen that

$$\left|\frac{\frac{bg}{K}\frac{\partial}{\partial x}(\overline{\eta^2})}{\frac{2H}{K}\frac{\partial}{\partial y}\Big(\overline{u\frac{\partial u}{\partial x}}\Big)}\right| \sim \frac{B_0^2}{a^2}, \tag{4.2.44}$$

where $a = \sqrt{gH}/f$ is the barotropic Rossby radius. From (4.2.44) we see that to neglect the last term in (4.2.41) the condition that has to be fulfilled is that $B_0^2/a^2 \ll 1$. This is exactly the same condition as in (2.1.21) on page 8, which we have already found to hold. Using (4.2.18) and (4.2.19) and neglecting the last term, (4.2.41) then becomes

$$\begin{aligned}&\frac{2fb}{K}\bar{V}_E + \frac{\partial \bar{U}_E}{\partial y} - 2b\bar{U}_E = \\ &\quad\frac{u_0^2 H_1\alpha}{K}\, e^{-2\alpha x}\left[l\sin(2ly) + b\left(\frac{l^2+b^2+k^2}{k^2}\right)\big(\cos(2ly) - 1\big)\right]\end{aligned} \tag{4.2.45}$$

Since $\bar{U}_S$ is known, $\bar{V}_E$ in (4.2.45) can be related to $\bar{U}_E$ through the continuity equation (4.2.34). Hence, taking $\frac{\partial}{\partial y}$(4.2.45) we find for $\bar{U}_E$ that

$$\begin{aligned}\frac{\partial^2 \bar{U}_E}{\partial y^2} - 2b\frac{\partial \bar{U}_E}{\partial y} - \frac{2fb}{K}\frac{\partial \bar{U}_E}{\partial x} = \frac{2fb}{K}\frac{\partial \bar{U}_S}{\partial x} \\ + \frac{2u_0^2 H_1 \alpha}{K} e^{-2\alpha x}\left[l^2\cos(2ly) - bl\left(\frac{l^2+b^2+k^2}{k^2}\right)\sin(2ly)\right]\end{aligned} \tag{4.2.46}$$

From the dispersion relation (4.2.16) it can be seen, for the last term in (4.2.46), that

$$bl\left(\frac{l^2+b^2+k^2}{k^2}\right) = \frac{2fb^2 l}{k\omega} \tag{4.2.47}$$

Assuming that

$$\bar{U}_E = e^{-2\alpha x}F(y), \tag{4.2.48}$$

inserting into (4.2.46) and using that $\bar{U}_S$ is given by (4.2.22), we then obtain a differential equation for F:

$$\begin{aligned}F'' - 2bF' + \frac{4fb\alpha}{K}F = \\ \frac{2u_0^2 H_1 \alpha}{K}\Big[\left(l^2 - \frac{2fbl^2}{k\omega}\right)\cos(2ly) - \frac{3fb^2 l}{k\omega}\sin(2ly)\Big]\end{aligned} \tag{4.2.49}$$

Ideally the boundary condition would be vanishing volume flux far away from the coast, i.e. as $y \to \infty$, but since the right hand side of (4.2.49) is only valid for $0 \le y \le B_0$, this cannot be used here (recall that the linear equations are restricted to the shelf area). From the frictionless problem in chapter 4.1 we know, however, that the amplitude of the shelf waves is exponentially trapped against the shelf. Since this must apply here as well, we know that the volume flux must decay rapidly from the shelf edge and further offshore, and as boundary conditions we will simply assume that

$$\bar{U}_E = -\bar{U}_S, \quad y = B_0 \tag{4.2.50}$$

$$\frac{\partial \bar{U}_E}{\partial y} = -\frac{\partial \bar{U}_S}{\partial y}, \quad y = B_0 \tag{4.2.51}$$

Since (4.2.49) has constant coefficients, it is easy to solve. The homogeneous solution is on the form

$$F_h \sim Ce^{\lambda_1}, \tag{4.2.52}$$

where

$$\lambda_1 = b \pm \sqrt{b^2 - \frac{4fb\alpha}{K}} \tag{4.2.53}$$

With the assumption that $O(K) \sim O(r)$, it can be seen from (4.2.17) that λ_1 will, for most wavenumbers, be complex. A general homogeneous solution is then

$$F_h = e^{by}\big(C_1\cos(qy) + C_2\sin(qy)\big), \tag{4.2.54}$$

where C_1 and C_2 are constants that can be determined by the boundary conditions and

$$q = \sqrt{\left| b^2 - \frac{4fb\alpha}{K} \right|} \tag{4.2.55}$$

The particular solution to (4.2.49) is

$$F_p = \frac{u_0^2 H_1 k}{2\omega}\big(A\sin(2ly) - B\cos(2ly)\big), \tag{4.2.56}$$

and it can be seen by insertion into (4.2.49) that the dimensionless constants A and B are given by

$$\begin{aligned} A &= \frac{\alpha l b\left(4l^2 fbK - 3f^2b^2\alpha - l^2Kk\omega\right)}{k^2\left(l^4K^2 - 2l^2Kfb\alpha + f^2b^2\alpha^2 + b^2l^2K^2\right)} \\ B &= \frac{\alpha l^2\left(3fb^3K + f^2b^2\alpha + l^2Kk\omega - l^2K(fb - k\omega) - fb\alpha k\omega\right)}{k^2\left(l^4K^2 - 2l^2Kfb\alpha + f^2b^2\alpha^2 + b^2l^2K^2\right)} \end{aligned} \tag{4.2.57}$$

Adding (4.2.54) and (4.2.56) we find that the total solution is given by

$$F = e^{by}\big(C_1\cos(qy) + C_2\sin(qy)\big) + \frac{u_0^2 H_1 k}{2\omega}\big(A\sin(2ly) - B\cos(2ly)\big) \tag{4.2.58}$$

With $\bar{U}_S$ given by (4.2.22) and $\bar{U}_E$ from (4.2.48), the first boundary condition (4.2.50) gives us the equation

$$\begin{aligned} &C_1\cos(qy) + C_2\sin(qy) = -\frac{u_0^2 H_1 k}{2\omega}e^{-bB_0} \\ &\cdot\left[\frac{bl\sin(2lB_0) + l^2\cos(2lB_0)}{k^2} + A\sin(2lB_0) - B\cos(2lB_0)\right] \end{aligned} \tag{4.2.59}$$

Using the transcendental equation (4.2.13), we can find that

$$\frac{bl\sin(2lB_0) + l^2\cos(2lB_0)}{k^2} = -\frac{l^2}{k^2}, \tag{4.2.60}$$

which inserted into (4.2.59) gives

$$C_1\cos(qy) + C_2\sin(qy) = \frac{u_0^2 H_1 k}{2\omega}e^{-bB_0}\left[\frac{l^2}{k^2} - A\sin(2lB_0) + B\cos(2lB_0)\right] \tag{4.2.61}$$

Similarly, the second boundary condition (4.2.51) yields

$$\begin{aligned} &-C_1 q\sin(qB_0) + C_2 q\cos(qB_0) + b\big[C_1\cos(qB_0) + C_2\sin(qB_0)\big] = \\ &-\frac{u_0^2 H_1 kl}{\omega}e^{-bB_0}\left[\frac{bl\cos(2lB_0) - l^2\sin(2lB_0)}{k^2} + A\cos(2lB_0) + B\sin(2lB_0)\right] \end{aligned} \tag{4.2.62}$$

Together, the two equations (4.2.61) and (4.2.62) can be used to determine the two constants C_1 and C_2:

$$\begin{aligned} C_1 &= \frac{u_0^2 H_1 k}{2\omega} D \\ C_2 &= \frac{u_0^2 H_1 k}{2\omega} E \end{aligned} \tag{4.2.63}$$

where D and E are dimensionless constants given by

$$\begin{aligned} D = \frac{e^{-bB_0}}{qk^2}\Big[& 2\,l^2 b\cos(2\,lB_0)\sin(qB_0) - 2\,l^3\sin(2\,lB_0)\sin(qB_0) \\ & + 2\,lA\cos(2\,lB_0)\,k^2\sin(qB_0) + 2\,lB\sin(2\,lB_0)\,k^2\sin(qB_0) \\ & + b\sin(qB_0)\,B\cos(2\,lB_0)\,k^2 + b\sin(qB_0)\,l^2 \\ & - b\sin(qB_0)\,A\sin(2\,lB_0)\,k^2 + q\cos(qB_0)\,B\cos(2\,lB_0)\,k^2 \\ & + q\cos(qB_0)\,l^2 - q\cos(qB_0)\,A\sin(2\,lB_0)\,k^2\Big] \\ E = -\frac{e^{-bB_0}}{qk^2}\Big[& - qB\cos(2\,lB_0)\,k^2\sin(qB_0) - ql^2\sin(qB_0) \\ & + qA\sin(2\,lB_0)\,k^2\sin(qB_0) + \cos(qB_0)\,bB\cos(2\,lB_0)\,k^2 \\ & + \cos(qB_0)\,bl^2 - \cos(qB_0)\,bA\sin(2\,lB_0)\,k^2 \\ & + 2\,\cos(qB_0)\,l^2 b\cos(2\,lB_0) - 2\,\cos(qB_0)\,l^3\sin(2\,lB_0) \\ & + 2\,\cos(qB_0)\,lA\cos(2\,lB_0)\,k^2 + 2\,\cos(qB_0)\,lB\sin(2\,lB_0)\,k^2\Big] \end{aligned} \tag{4.2.64}$$

Since the expressions for the constants are rather long we will simply let the solution to F be represented by

$$F = \frac{u_0^2 H_1 k}{2\omega}\Big[e^{by}\left(D\cos(qy) + E\sin(qy)\right) + A\sin(2ly) - B\cos(2ly)\Big], \tag{4.2.65}$$

keeping in mind that q, A, B, D and E are given by the equations (4.2.55), (4.2.57) and (4.2.64). From (4.2.48) the mean Eulerian volume flux along the coast is then given by

$$\bar{U}_E = \frac{u_0^2 H_1 k}{2\omega} e^{-2\alpha x}\Big[e^{by}\left(D\cos(qy) + E\sin(qy)\right) + A\sin(2ly) - B\cos(2ly)\Big] \tag{4.2.66}$$

From the results so far we see that due to friction, there is an induced mean Eulerian flux that is of the same order as the Stokes flux. This is analog to what Weber (2009) found for coastal Kelvin waves. The total

mean Lagrangian flux now becomes

$$\bar{U}_L = \frac{u_0^2 H_1 k}{2\omega} e^{-2\alpha x}\left[\frac{bl\sin(2ly) + l^2\cos(2ly)}{k^2} + e^{by}\left(D\cos(qy) + E\sin(qy)\right) + A\sin(2ly) - B\cos(2ly)\right] \tag{4.2.67}$$

With the Lagrangian flux decaying along the coast, the flow field must obviously be divergent, which means that there must be a volume flux $\bar{V}_L = \bar{V}_E \neq 0$. Finding $\bar{V}_E$ can be done by integrating the continuity equation. From (4.2.34) we have that

$$\frac{\partial \bar{V}_E}{\partial y} = -\frac{\partial \bar{U}_E}{\partial x} - \frac{\partial \bar{U}_S}{\partial x} \tag{4.2.68}$$

Since there can be no volume flux into the coast, and since $\bar{V}_S = 0$, the boundary condition for $\bar{V}_E$ must be that

$$\bar{V}_E = 0, \quad y = 0 \tag{4.2.69}$$

Integrating (4.2.68) with respect to y, with $\bar{U}_S$ from (4.2.22), $\bar{U}_E$ from (4.2.66) and using the boundary condition (4.2.69), $\bar{V}_E$ becomes

$$\begin{aligned}\bar{V}_E =& \frac{u_0^2 H_1 \alpha}{2\omega} e^{-2\alpha x}\left[\frac{l\sin(2ly) - b\big(\cos(2ly) - 1\big)}{k}\right. \\ &+ \frac{k}{l\left(b^2+q^2\right)}\left\{ - A\left(b^2+q^2\right)\left(\cos\left(2\,ly\right) - 1\right)\right. \\ &- B\left(b^2+q^2\right)\sin\left(2\,ly\right) + 2\,l\Big[\,(Db - Eq) \\ &\left.\left.\left(\cos\left(qy\right) - 1\right) + \sin\left(qy\right)(Dq + Eb)\,\Big]\left(e^{by} - 1\right)\right\}\right]\end{aligned} \tag{4.2.70}$$

Hence, there is a small flux ($O(\alpha)$) in the direction perpendicular to the coast. Dividing (4.2.67) by the depth $H = H_1 e^{2by}$ we find the mean wave-induced particle velocity in the longshore direction:

$$\bar{u}_L = \frac{u_0^2 k}{2\omega} e^{-2\alpha x - 2by}\left[\frac{bl\sin(2ly) + l^2\cos(2ly)}{k^2} + e^{by}\left(D\cos(qy) + E\sin(qy)\right) + A\sin(2ly) - B\cos(2ly)\right] \tag{4.2.71}$$

The first term in (4.2.71) is the Stokes drift, and the other terms represent the mean Eulerian drift, $\bar{u}_E$. So far it has only been assumed that the

frictional effect on the waves and on the mean flow are of the same order, i.e. $O(r) \sim O(K)$. Now, for simplicity, let us assume that they are exactly the same, i.e. that $K = r$. Inserting from equation (4.2.17) into (4.2.57) and (4.2.55) it can then be seen that we loose all the terms with α in A, B and q, and the drift can be determined from the values of k, b, l, B_0 and f. Consider a wave of 1500 km, and let values of f, B_0 and b be the same as in chapter 3, i.e.

$$\begin{aligned} &k = \frac{2\pi}{1500 \text{ km}}, \quad B_0 = B_2 = 155 \text{ km} \quad f = 1.3 \cdot 10^{-4} \text{ s}^{-1}, \\ &2b = 1.49 \cdot 10^{-5} \text{ m}^{-1} \end{aligned} \tag{4.2.72}$$

From the discussion above, all the other parameters can then be calculated. As in chapter 4.1, we will consider the first mode, and the resulting longshore drift is scaled by the maximum Stokes drift (at the coast) and plotted against the distance from the shore in figure 4.4 below.

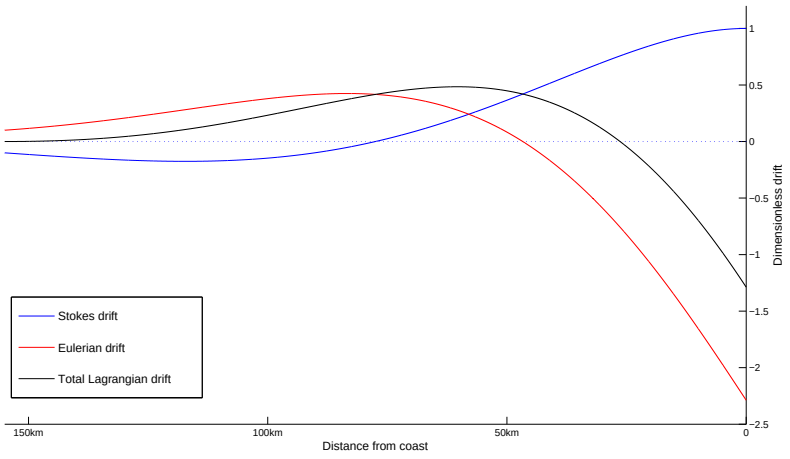

Figure 4.4: The scaled Stokes drift, Eulerian drift and total Lagrangian drift induced by the first mode plotted against the distance from the coast. The wavelength is 1500 km

Figure 4.4 illustrates that the Eulerian drift is of the same order of magnitude as the Stokes drift.
Let us consider an example of the drift, as in chapter 4.1.2, but for a wave of 1500 km. Using (4.2.18) we can find that an observed velocity amplitude of 0.5 ms^{-1} at the coast, assuming we are at $x = 0$, would mean that

$$|u_0| = 0.16 \text{ ms}^{-1} \tag{4.2.73}$$

From (4.2.21) and (4.2.71), at $y = 0$, we then have that

$$\bar{u}_S = 1.63 \text{ cm s}^{-1}, \quad \bar{u}_E = -3.74 \text{ cm s}^{-1}, \quad \bar{u}_L = -2.11 \text{ cm s}^{-1} \quad (4.2.74)$$

4.3 Results and discussion

We started this chapter by finding expressions for the Stokes drift over the three different shelf models introduced in chapter 3. When applying the exponential shelf profile, the variation over the shelf was harder to see from the expressions, so the scaled Stokes drift over the shelves induced by two different wavelengths was plotted. For the continental shelf only the drift induced by the first wave mode was considered, since it is expected to be dominating, and since all the modes seem to behave similarly from the dispersion diagram. For the interior shelf, the Stokes drift was plotted for the two first modes, since we found that they have rather different dispersion diagrams in chapter 3.2.
In all the plots, the Stokes drift was scaled by the maximum magnitude, so that they only show the relative distribution over the shelf region. These results reveal that the different models of the shelf profile change the structure of the Stokes drift over the shelf. With the step-shelf, the drift is always in the positive x-direction, and becomes greater from the coast towards the step, where it is the greatest. Over the deep ocean there is, in this case, no Stokes drift at all.

Over the exponential shelf, the Stokes drift changes in direction across the shelf. It has the greatest magnitude at the coast, and is in the positive x-direction, while it decreases in magnitude and changes sign towards the base of the continental slope. Over the deep ocean the Stokes drift is very small compared to the value at the coast, and dies out exponentially. As an example, the theoretical magnitude of the Stokes drift at the coast, induced by the first mode, was calculated for two different wavelengths. Ideally the velocity amplitudes should come from real observations, but since (to my knowledge) no such measurements exist for the Norwegian shelf, an estimate of a wave-induced velocity amplitude of 0.5 ms^{-1} was made, based on results from Martinsen et al. (1979) and Gill and Schumann (1974). The resulting value of the Stokes drift at the coast may, however, give us an idea of what magnitudes one could expect.

In the second part of this chapter, the effect of friction was taken into account. First a simple Rayleigh friction was introduced in the linearized momentum equation, and a damped version of the vorticity equation was derived. Assuming that the damping coefficient was small, and restricting the analysis to long waves, we then found damped solutions of the velocities, the surface elevation and the Stokes flux over the exponential shelf.

Vertically integrating the momentum and continuity equation, a set of equations for the horizontal fluxes, exact under the Boussinesq approximation, were introduced. This set of equations was simplified assuming hydrostatic pressure distribution, no forcing from the wind or the pressure at the surface and expressing the friction force components in terms of the horizontal frictional shear stresses. Averaging over a wave period, we arrived at three equations where all the wave forcing terms could be determined, to second order in wave amplitude, by the linear solutions of the velocities and the surface elevation. Solving this set of equations, we arrived at expressions for the mean Eulerian volume fluxes, and hence the total Lagrangian drift could be determined.

Finally, considering the first mode of a wave of 1500 km, the Stokes drift, the Eulerian drift and the total Lagrangian drift were scaled and plotted against the distance from the coast. The Stokes drift and the longshore Eulerian drift were of similar magnitude, both greatest at the coast, but oppositely directed. As an example, $\bar{u}_S$, $\bar{u}_E$, and $\bar{u}_L$ at the coast were calculated for this wavelength, assuming the same velocity amplitude at the coast as in the first part of the chapter.

Chapter 5

Summary and Conclusions

The main purpose of this thesis has been to study the drift induced by continental shelf waves along the western coast of Norway. Working with analytical solutions, the coast was assumed straight, and two different shelf profiles were considered.

Basic equations

A set of equations governing the motion was derived, based on shallow water theory for a uniformly rotating, homogeneous ocean. The rigid lid approximation was also used, and was found to hold for shelf waves provided that the shelf width is much smaller than the external Rossby radius. From the governing equations the vorticity equation was derived, and using the conservation of potential vorticity theorem, the mechanism for propagation was discussed.

The shelf profile

In order to find wave solutions, two different shelf profiles were considered. Applying a step topography, only one wave mode could exist, and the phase and group velocity are always in the same direction. Using an exponential shelf gave rise to an infinite (discrete) number of wavemodes, for which the dispersion curves show similar behaviour.
The propagation of shelf waves along the interior shelf to the North of Norway was also investigated. In this case, when there was no coastal boundary, the dispersion curve for the first mode showed a different behaviour than the higher modes.

Wave induced currents

Working with classical Stokes theory, the Stokes drift induced by the waves

over the different shelves was found. The variation of the Stokes drift proved to be different for the two shelf profiles. Over the step shelf the Stokes drift was increasing exponentially from the coast towards the shelf edge, while in the case of an exponential shelf the Stokes drift fluctuated between being in the positive and negative longshore direction.
Including friction in the linearized shallow water equations, damped solutions of the velocities and the surface elevation were found, valid for long waves. Considering steady mean flow, a nonlinear, inhomogeneous set of equations for the mean Eulerian volume flux and the mean surface elevation was then derived. The wave-forcing terms in this set of equations could be determined by the linear damped solutions found earlier, to second order accuracy in wave amplitude. Solving for the mean Eulerian volume flux a general expression for the total Lagrangian drift was found.

Although only valid for long waves, and under several restricting approximations, the variation of the total Lagrangian drift over the shelf may give insight into the general circulation over the shelf. Even though the estimate of a velocity amplitude of 0.5 ms^{-1} may not be realistic, the resulting magnitudes of the Stokes drift, the Eulerian drift and the total Lagrangian drift show that the mean currents induced by shelf waves along the western coast of Norway might be significant.

Future work

From the results in this thesis, it is clear that there are several topics regarding the dynamics of shelf waves over the Norwegian shelf that should be investigated. Some ideas for future work are listed below.

- Redo the analysis of chapter 4.2, without the longwave assumption. One could, for instance, study the other extreme, i.e. short waves, and use a boundary conditions of zero normal velocities at both the coast and the shelf edge. It would also be interesting to parametrize the friction differently.
- Apply actual measurements of the velocity amplitudes at the coast in the results of this thesis.
- Model the shelf waves and investigate the wave-induced mass transport numerically, to resolve the variation of the coastline and the shelf in a more realistic way.

Appendix A

The first mode of the Interior shelf

It can be seen from (3.2.24) that for the first mode, and for real $\hat{l}$, $\hat{k}$ has a minimum value $\hat{k}_0 > 0$ that occurs in the limit $\hat{l} \to 0$. From the third order Taylor expansion on both sides of (3.2.24) about $l = 0$ we get that

$$\hat{l} + \frac{1}{3}\hat{l}^3 = \frac{2\hat{k}}{\hat{b}^2 - \hat{k}^2}\hat{l} - \frac{2\hat{k}}{\left(\hat{b}^2 - \hat{k}^2\right)^2}\hat{l}^3 \tag{A .1}$$

$$\Leftrightarrow \quad 1 + \frac{1}{3}\hat{l}^2 = \frac{2\hat{k}}{\hat{b}^2 - \hat{k}^2} - \frac{2\hat{k}}{\left(\hat{b}^2 - \hat{k}^2\right)^2}\hat{l}^2 \tag{A .2}$$

From (A .2), with $\hat{l} = 0$ and $\hat{k} = \hat{k}_0$, we see that

$$\frac{2\hat{k}_0}{\hat{b}^2 - \hat{k}_0^2} = 1, \tag{A .3}$$

so that

$$\hat{k}_0 = \sqrt{1 + \hat{b}^2} - 1 \tag{A .4}$$

is the minimum value of $\hat{k}$.
However, if we let $\hat{l} = i\hat{p}$, (3.2.24) changes to

$$\tanh(\hat{p}) = \frac{2\hat{k}\hat{p}}{\hat{b}^2 - \hat{k}^2 - \hat{p}^2} \quad , \tag{A .5}$$

which has a root for $\hat{p}$ in the range $0 \leq \hat{p} < \hat{b}$, if and only if $\hat{k}_0 \geq \hat{k} \geq 0$ (Buchwald and Adams, 1968). This means that the first mode does cover the full range of $\hat{k}$, but $\hat{l}$ is complex for $\hat{k} < \hat{k}_0$. To satisfy (A .5) when $\hat{k} \to 0$, we must have that

$$\hat{p} \to \hat{b} - C\hat{k} \quad as \quad \hat{k} \to 0, \tag{A .6}$$

where C is a constant. Using this, we then find from (A .5), as $\hat{k} \to 0$, that

$$C = \coth(\hat{b}) \tag{A .7}$$

Inserting (A .7) into (A .6), we find that

$$\hat{k} = (\hat{b} - \hat{p}) \tanh(\hat{b}), \quad as \quad \hat{k} \to 0 \tag{A .8}$$

Now, writing (3.2.23) on the same form as in (3.1.48), with $\hat{l} = i\hat{p}$ we have for the first mode that

$$\sigma_1 = \frac{2\hat{b}\hat{k}}{\hat{k}^2 - \hat{p}^2 + \hat{b}^2} \to \tanh(\hat{b}) \quad as \quad \hat{k} \to 0 \tag{A .9}$$

From (A .9) we see that the frequency tends to a fixed limit as $\hat{k} \to 0$, which means that the phase velocity becomes very large for long wavelengths.
It still remains to investigate what happens to σ_1 in the transition from real to complex $\hat{l}$, where $\hat{k}$ is close to $\hat{k}_0$. For $\hat{k}$ slightly larger than $\hat{k}_0$, $\hat{l}$ is real and given by (3.2.24). Using Taylor expansion about $\hat{l} = 0$ of the left hand side of (3.2.24) then gives us, to third order in $\hat{l}$, that

$$\hat{l} + \frac{1}{3}\hat{l}^3 = \frac{2\hat{k}\hat{l}}{\hat{l}^2 + \hat{b}^2 - \hat{k}^2}, \tag{A .10}$$

or, by rearranging:

$$\frac{1}{3}\hat{l}^2 = \frac{2\hat{k}}{\hat{l}^2 + \hat{b}^2 - \hat{k}^2} - 1 \tag{A .11}$$

Consider

$$\hat{k} = \hat{k}_0 + \Delta\hat{k}, \tag{A .12}$$

where $\Delta\hat{k}$ is small. (A .12) into (A .11) then gives

$$\frac{1}{3}\hat{l}^2 = \frac{2\hat{k}_0\left(1 + \frac{\Delta\hat{k}}{\hat{k}_0}\right)}{(\hat{b}^2 - \hat{k}_0^2)\left(1 + \frac{1}{\hat{b}^2 - \hat{k}_0^2}(\hat{l}^2 - 2\hat{k}_0\Delta\hat{k})\right)} - 1 \tag{A .13}$$

where terms of $O(\Delta\hat{k}^2)$ have been neglected since they are very small. Using (A .3), (A .13) can be written

$$\frac{1}{3}\hat{l}^2 = \frac{1 + \frac{\Delta\hat{k}}{\hat{k}_0}}{1 + \frac{1}{2\hat{k}_0}(\hat{l}^2 - 2\hat{k}_0\Delta\hat{k})} - 1 \tag{A .14}$$

Assuming that $\hat{l}^2 \sim \Delta\hat{k}$, the term $\frac{1}{2\hat{k}_0}(\hat{l}^2 - 2\hat{k}_0\Delta\hat{k})$ in (A .14) is small, and (A .14) can be approximated by

$$\frac{1}{3}\hat{l}^2 = \left(1 + \frac{\Delta\hat{k}}{\hat{k}_0}\right)\left(1 - \frac{1}{2\hat{k}_0}(\hat{l}^2 - 2\hat{k}_0\Delta\hat{k})\right) - 1 \tag{A .15}$$

Solving (A .15) for $\hat{l}^2$ we then get, to $O(\Delta\hat{k})$, that

$$\hat{l}^2 = \frac{6(\hat{k}_0+1)}{2\hat{k}_0+3}\Delta\hat{k} \tag{A .16}$$

Using (A .16) we get, again to $O(\Delta\hat{k})$, that

$$\sigma_1(\hat{k}_0+\Delta\hat{k}) = \frac{2\hat{b}(\hat{k}_0+\Delta\hat{k})}{\hat{b}^2+\hat{k}_0^2+2\hat{k}_0\Delta\hat{k}+\frac{6(\hat{k}_0+1)}{2\hat{k}_0+3}\Delta\hat{k}}, \tag{A .17}$$

which can be expressed in terms of $\sigma_1(\hat{k}_0)$:

$$\sigma_1(\hat{k}_0+\Delta\hat{k}) = \sigma_1(\hat{k}_0)\frac{1+\frac{\Delta\hat{k}}{\hat{k}_0}}{1+\frac{2\hat{k}_0}{\hat{b}^2+\hat{k}_0^2}\left(1+\frac{3(\hat{k}_0+1)}{\hat{k}_0(2\hat{k}_0+3)}\right)\Delta\hat{k}} \tag{A .18}$$

Using (A .3) in (A .18) we get that

$$\sigma_1(\hat{k}_0+\Delta\hat{k}) = \sigma_1(\hat{k}_0)\frac{1+\frac{\Delta\hat{k}}{\hat{k}_0}}{1+\frac{\hat{k}_0(2\hat{k}_0+3)+3(\hat{k}_0+1)}{\hat{k}_0(1+\hat{k}_0)(2\hat{k}_0+3)}\Delta\hat{k}} \tag{A .19}$$

Since $\Delta\hat{k}$ is small, (A .19) is approximately given by

$$\begin{aligned}&\sigma_1(\hat{k}_0+\Delta\hat{k}) = \\ &\sigma_1(\hat{k}_0)\left(1+\frac{\Delta\hat{k}}{\hat{k}_0}\right)\left(1-\frac{\hat{k}_0(2\hat{k}_0+3)+3(\hat{k}_0+1)}{\hat{k}_0(1+\hat{k}_0)(2\hat{k}_0+3)}\Delta\hat{k}\right),\end{aligned} \tag{A .20}$$

which, to $O(\Delta\hat{k})$, gives us that

$$\sigma_1(\hat{k}_0+\Delta\hat{k}) = \sigma_1(\hat{k}_0)\left[1-\frac{\Delta\hat{k}}{(1+\hat{k}_0)(2\hat{k}_0+3)}\right] \tag{A .21}$$

From (A .21) it is clear that the value of σ_1 is decreasing for increasing $\Delta\hat{k}$. Since $\Delta\hat{k}$ can be infinitely small, σ_1 must be monotonely decreasing from the point $\hat{k}=\hat{k}_0$ onwards.

For $\hat{k}$ slightly smaller than $\hat{k}_0$, i.e. $\hat{k}=\hat{k}_0-\Delta\hat{k}$, $\hat{l}=i\hat{p}$ is complex and given by (A .5). Following the same steps as was done in the case of $\hat{k}=\hat{k}_0+\Delta\hat{k}$, we may use the Taylor expansion of the left hand side of (A .5) about $\hat{p}=0$, and get that

$$\frac{1}{3}\hat{p}^2 = 1-\frac{2\hat{k}}{\hat{p}^2-\hat{k}^2-\hat{p}^2} \tag{A .22}$$

With $\hat{k} = \hat{k}_0 - \Delta\hat{k}$, to $O(\Delta\hat{k})$, using (A .3) we then get that

$$\frac{1}{3}\hat{p}^2 = 1 - \frac{1 - \frac{\Delta\hat{k}}{\hat{k}_0}}{1 + \frac{1}{2\hat{k}_0}\left(2\hat{k}_0\Delta\hat{k} - \hat{p}^2\right)} \tag{A .23}$$

Assuming $\hat{p} \sim \Delta\hat{k}$, the second term in the denominator of (A .23) is small, and exept for a very small extra term we have that

$$\frac{1}{3}\hat{p}^2 = 1 - \left(1 - \frac{\Delta\hat{k}}{\hat{k}_0}\right)\left(1 - \frac{1}{2\hat{k}_0}(2\hat{k}_0\Delta\hat{k} - \hat{p}^2)\right) \tag{A .24}$$

From (A .24), to $O(\Delta\hat{k})$, it is then easy to find that

$$\hat{p}^2 = \frac{6(\hat{k}_0 + 1)}{2\hat{k}_0 + 3}\Delta\hat{k}, \tag{A .25}$$

which is identical to $\hat{l}^2$ in (A .16). In this case we have that

$$\sigma_1 = \frac{2\hat{b}\hat{k}}{\hat{b}^2 + \hat{k}^2 - \hat{p}^2} \tag{A .26}$$

With $\hat{k} = \hat{k}_0 - \Delta\hat{k}$, using (A .3) and to $O(\Delta\hat{k})$ (A .26) becomes

$$\sigma_1(\hat{k} - \Delta\hat{k}) = \sigma_1(\hat{k}_0)\frac{1 - \frac{\Delta\hat{k}}{\hat{k}_0}}{1 - \frac{\hat{k}_0(2\hat{k}_0+3)+3(\hat{k}_0+1)}{\hat{k}_0(1+\hat{k}_0)(2\hat{k}_0+3)}\Delta\hat{k}}, \tag{A .27}$$

which, since $\Delta\hat{k}$ is small, is approximately equivalent to

$$\begin{aligned}&\sigma_1(\hat{k}_0 - \Delta\hat{k}) = \\ &\sigma_1(\hat{k}_0)\left(1 - \frac{\Delta\hat{k}}{\hat{k}_0}\right)\left(1 + \frac{\hat{k}_0(2\hat{k}_0 + 3) + 3(\hat{k}_0 + 1)}{\hat{k}_0(1 + \hat{k}_0)(2\hat{k}_0 + 3)}\Delta\hat{k}\right)\end{aligned} \tag{A .28}$$

To $O(\Delta\hat{k})$ (A .28) becomes

$$\sigma_1(\hat{k}_0 - \Delta\hat{k}) = \sigma_1(\hat{k}_0)\left[1 + \frac{\Delta\hat{k}}{(1 + \hat{k}_0)(2\hat{k}_0 + 3)}\right] \tag{A .29}$$

From (A .29) it is obvious that $\sigma_1(\hat{k})$, when $\hat{k} = \hat{k}_0 - \Delta\hat{k}$, increases for increasing $\Delta\hat{k}$, and therefore σ_1 must be monotonely decreasing with $\hat{k}$ also on this side of $\hat{k} = \hat{k}_0$. Since (A .21) and (A .29) both converge to the same value of σ_1 as $\Delta\hat{k} \to 0$ it is also obvious that σ_1 is continous and monotonely decreasing with $\hat{k}$ through the point $\hat{k} = \hat{k}_0$. σ_1 also decreases at the same rate on both sides of$\hat{k}_0$, and hence the graph of σ_1 has no salient point at $\hat{k} = \hat{k}_0$.

Bibliography

Adams, J. K. and Buchwald, V. T. (1969) *T*he generation of continental shelf waves. Journal of Fluid Mechanics, Vol. 35: p. 815–826.

Buchwald, V. T. and Adams, J. K. (1968) *T*he Propagation of Continental Shelf Waves. Proceedings of the Royal Society of London. Series A,Mathemati cal and Physical Sciences, Vol. 305, No. 1481: p. 235–250.

Gill, A. E. (1982) *A*tmosphere-Ocean Dynamics (Academic Press).

Gill, A. E. and Schumann, E. H (1974) *T*he generation of long shelf waves by the wind. Journal of Physical Oceanography, Vol. 4: p. 83–90.

LeBlond, Paul H. and Mysak, Lawrence A. (1978) *W*aves in The Ocean (Elsevier Scientific Publishing Company).

Longuet-Higgins, M. S. (1953) *M*ass transport in water waves. Philosophical Transactions of the Royal Society of London. Series A, Mathematical and Physical Sciences, Vol. 245, No. 903: p. 535–581.

Longuet-Higgins, M. S. (1965) *S*ome dynamical aspects of ocean currents. Quarterly Journal of the Royal Meteorological Society, Vol. 91(390): p. 425–451.

Martinsen, E. A.; Gjevik, Bjørn and Røed, Lars Petter (1979) *A* numerical model for long barotropic waves and storm surges along the western coast of Norway. Journal of Physical Oceanography, Vol. 9: p. 1126–1138.

Mysak, Lawrence A. (1980a) *T*opographically trapped waves. In *A*nn. Rev. Fluid Mech., Vol. 12, p. 45–76 (Annual Reviews Inc.).

Mysak, Lawrence A. (1980b) *R*ecent advances in shelf wave dynamics. In *R*eviews of Geophysics and Space physics, Vol. 18, p. 211–241 (American Geophysical Union).

Stokes, G. G. (1847) *O*n the theory of oscillatory waves. Trans. Camb. Phil. Soc., Vol. 8: p. 441–445.

Weber, Jan Erik H. (2009) *GEF 4610 -Dynamic Oceanography: Waves and wave-induced mass transport in the ocean.* Department of Geosciences, Section for Meteorology and Oceanography, University of Oslo.